

**Li-ion Battery State of Charge (SOC) and State of Health (SOH) Online  
Estimations Using Partial Charge or Discharge Data**

by

Amin Bavand

A thesis submitted in partial fulfillment of the requirements for the degree of

Master of Science

in

Software Engineering and Intelligent Systems

Department of Electrical and Computer Engineering  
University of Alberta

© Amin Bavand, 2021

# Abstract

Estimating the state of health (SOH) and state of charge (SOC) of Lithium-ion (Li-ion) batteries is crucial for lifetime and performance optimizations. Many existing online estimation methods are not practical in many applications as they may need offline training, take too much time for estimations, or need a full discharge or charge cycle for accurate results. In this thesis, a fast online SOH/SOC estimation method for batteries with partial charge/discharge condition is introduced that can provide accurate results in various operating and temperature conditions.

First, a method for online estimation of SOH/SOC is introduced. Based on only two consecutive partial discharge intervals, the battery equivalent circuit model (ECM) parameters and the open circuit voltage (OCV) relation with the battery charge are estimated using Adam optimization algorithm. By comparing the estimated OCV curve at each interval with the reference OCV curve of the brand new battery, the battery capacity and therefore its SOH along with SOC are estimated.

In many applications the temperature changes in a wide range that may create relatively large errors in state estimations. The proposed method is further refined to guarantee accurate results and estimations in various temperature conditions. In this modification, the SOC-OCV curve is extracted from the battery datasheet and is predicted for different temperatures, which are then used to estimate SOH/SOC at any given temperature.

In this thesis, the proposed methods are validated using NASA dataset. The proposed method results in root mean square error (RMSE) below 1% for SOH and 1.07% for SOC on average. Moreover, it is shown that using the refined method, the

SOH estimation RMSE is improved by 2.55% when the datasheet's SOC-OCV curves are adjusted according to their test temperatures.

# Preface

Some of the research conducted in this thesis is intended to be published. A journal article based on chapters 3 is in the process of submission.

# Acknowledgements

I would like to express my profound gratitude to my supervisors, Dr. Masoud Ardakani and Dr. Ali Khajehoddin for their endless support during my study. Without their guidance, this research would never be possible. I am grateful for the invaluable lessons they taught me and for their exceptional patience and care during editing my thesis.

I am also thankful to my friends who were always there for me in my good times and bad times. I am grateful for such wonderful friends whose encouragement and companionship made me capable of continuing my path.

Finally, I would like to thank my beloved family, for believing in me and always being there for me. I could never be where I am today without their endless love and support. I love them from the bottom of my heart and I would like to dedicate this thesis to them.

# Table of Contents

<b>1</b>	<b>Introduction</b>	<b>1</b>
1.1	Motivation . . . . .	1
1.2	Battery Management Systems (BMS) . . . . .	3
1.3	Thesis Overview . . . . .	4
<b>2</b>	<b>Background</b>	<b>7</b>
2.1	State Characterization for Li-ion Batteries . . . . .	7
2.1.1	State of Charge . . . . .	8
2.1.2	State of Health . . . . .	8
2.1.3	Depth of Discharge . . . . .	9
2.1.4	Remaining Useful Life . . . . .	9
2.2	Li-ion Battery Modeling . . . . .	9
2.2.1	The $R_{\text{int}}$ Model . . . . .	10
2.2.2	The RC Model . . . . .	10
2.2.3	The Thevenin Model . . . . .	11
2.2.4	The PNGV Model . . . . .	12
2.2.5	The DP Model . . . . .	13
2.2.6	Higher Order ECMs . . . . .	14
2.2.7	The Selected Model . . . . .	14
2.3	Adam Optimization Algorithm . . . . .	16
2.4	Neural Networks . . . . .	17
2.4.1	Neural Networks Training . . . . .	20

<b>3</b>	<b>The Proposed Method</b>	<b>21</b>
3.1	Introduction . . . . .	21
3.2	Problem Definition . . . . .	22
3.3	Basic Ideas and Assumptions . . . . .	24
3.3.1	$Q$ Variation is negligible in two consecutive intervals . . . . .	24
3.3.2	Normalized SOC-OCV does not change over the lifetime . . . . .	24
3.4	Details of the Proposed Method . . . . .	27
3.4.1	Partial Discharge Data Extraction . . . . .	27
3.4.2	$R_s$ Estimation . . . . .	28
3.4.3	$R_p$ , $C_p$ and OCV Estimation . . . . .	31
3.4.4	SOC-OCV curve and SOH Estimation . . . . .	32
3.5	Performance Evaluation . . . . .	32
3.5.1	Dateset and Verification Method . . . . .	32
3.5.2	Results and Discussion . . . . .	34
3.5.3	Estimation Error Evaluation for Partial Discharge Intervals . . . . .	40
3.5.4	Sensitivity Analysis . . . . .	41
3.6	Conclusion . . . . .	42
<b>4</b>	<b>Battery Status Estimation Considering Temperature</b>	<b>44</b>
4.1	Introduction . . . . .	44
4.2	Temperature Effect on Battery Parameters Estimation . . . . .	45
4.3	The Proposed Method . . . . .	49
4.3.1	Problem Definition . . . . .	49
4.3.2	Details of the Proposed Method . . . . .	51
4.3.3	Summary of the Proposed Method . . . . .	56
4.4	Estimation Results . . . . .	58
4.5	Conclusion . . . . .	58

<b>5</b>	<b>Conclusions and Future Work</b>	<b>62</b>
5.1	Summary of Works . . . . .	62
5.2	Future Work . . . . .	64
	<b>Bibliography</b>	<b>66</b>
	<b>Appendix A: Details of the Neural Network in Chapter 4</b>	<b>72</b>

# List of Tables

1.1	Comparison between characteristics of four different batteries [1] . . .	2
2.1	Adam optimization algorithm: $g_t^2$ indicates the element-wise square $g_t \odot g_t$ . Good default settings for the tested machine learning problems are $\alpha = 0.001, \beta_1 = 0.9, \beta_2 = 0.999$ and $\epsilon = 10^{-8}$ . All operations on vectors are element-wise [9]. . . . .	18
3.1	RMSE of the proposed method estimations . . . . .	37
3.2	Information regarding the dataset of the methods in literature [45] . .	38
3.3	Comparison between our proposed method and other methods in literature in terms of estimation RMSE, convergence time and initial capacity error(if applicable) for different types of datasets [45] . . . .	38
3.4	RMSE of SOC estimations . . . . .	40
4.1	RMSE of SOH estimations using reference SOC-OCV curve from the datasheet . . . . .	46
4.2	RMSE of SOH estimations using reference SOC-OCV curve from the datasheet for two cases: (i) without considering the effect of the temperature, (ii)with considering the effect of the temperature. Also, the SOH estimation RMSE improvement is reported in the last row. The first and the second rows indicate the battery number and the RMSE of temperature difference with 25°C for each battery respectively . . .	61

A.1	Summary of the parameters and results of the trained neural networks on batteries B14 and B15 . . . . .	73
-----	--	----

# List of Figures

1.1	Li-ion battery worldwide demand in electric vehicles and prediction for the next ten years [4] . . . . .	3
1.2	Li-ion battery pack cost prediction over the next ten years, based on Bloomberg New Energy Finance (BNEF) forecast [5], [6] . . . . .	4
1.3	BMS key features [8] . . . . .	5
2.1	Diagram of the $R_{int}$ model . . . . .	10
2.2	Diagram of the RC model . . . . .	11
2.3	Diagram of the Thevenin model . . . . .	12
2.4	Diagram of the PNGV model . . . . .	12
2.5	Diagram of the DP model . . . . .	13
2.6	Equivalent circuit model of order n for Li-ion batteries . . . . .	14
2.7	First order equivalent circuit model of Li-ion batteries . . . . .	15
2.8	A full discharge interval (a) Measured terminal voltage $V_T$ and (b) Measured load current $I_L$ profile. . . . .	16
2.9	SOC-OCV curve for a 18650 Li-ion battery [25] . . . . .	17
2.10	A fully connected neural network with three inputs, one output and two hidden layers with ten and three neurons respectively . . . . .	19
3.1	Flowchart of the proposed algorithm part 1 . . . . .	25
3.2	Flowchart of the proposed algorithm part 2 . . . . .	26
3.3	Flowchart of the proposed algorithm part 3 . . . . .	27
3.4	terminal voltage versus open circuit voltage in a discharge cycle. . . . .	29

3.5	Interval separation process: converting the raw signal into the desirable inputs. . . . .	30
3.6	(a) ISUM-OCV curves at three different aging levels. (b) SOC-OCV curves derived with normalizing ISUM-OCV curves by proper $Q$ at each aging level and reference SOC-OCV curve (black curve). . . . .	33
3.7	(a) Reference discharge profile for battery B3 (The curves fade from black to red as the battery ages. (b) Capacity fade curve for the battery B3. . . . .	34
3.8	SOH estimation curves (blue plots) vs real SOH curves (orange plots).	35
3.9	SOH estimation error curves. . . . .	36
3.10	SOC estimation curve for a sample discharge interval in NASA data.	40
3.11	SOH estimation error curves based on the length of the partial discharge intervals. . . . .	41
3.12	Sensitivity of SOH estimations to initial capacity ( $Q_{rated}$ ) error. . . . .	42
4.1	SOH estimation curves (blue plots) using datasheet's data at 25°C as the reference SOC-OCV curve vs reference SOH curves (orange plots).	47
4.2	SOH estimation error curves and temperatures using datasheet's data at 25°C as the reference SOC-OCV curve. . . . .	48
4.3	Datasheet discharge curves with different discharge currents at 25°C.	50
4.4	Datasheet discharge curves at different temperatures. . . . .	50
4.5	OCV curves estimations from the provided discharge curves in the datasheet as illustrated in Fig. 4.3. . . . .	52
4.6	The steady state internal resistance variation with temperature at 5 different SOC's for battery (a) B14, (b) B15. . . . .	54
4.7	The estimated SOC-OCV curves at 55°C and -20°C . . . . .	55
4.8	OCV variation for 1°C temperature increase . . . . .	56
4.9	Flowchart of the proposed algorithm . . . . .	57

4.10 SOH estimation curves (blue plots) using temperature compensated SOC-OCV curves vs reference SOH curves (orange plots). . . . .	59
4.11 SOH estimation error curves and temperatures. Error curves for both cases are drawn: (i)using the temperature compensated SOC-OCV curves (blue plots), (ii)using only one SOC-OCV curve for all temperatures (red plots) . . . . .	60
A.1 Neural network's structure. . . . .	72

# Chapter 1

## Introduction

### 1.1 Motivation

The 21st century is the era of modern technologies. Mobile and portable electronic devices such as electric vehicles (EV), cellular phones, laptops, tablets, digital cameras, power tools, audio devices, and gaming consoles are very commonly used in people's daily lives. These devices are rapidly growing and becoming more popular every day, both in personal and industrial use.

All these portable devices need energy sources in order to operate. Rechargeable batteries are commonly used as the energy source for these devices. Lead-acid, nickel-cadmium (Ni-Cd), nickel-metal hydride (Ni-MH), and lithium-ion (Li-ion) batteries are some examples of portable and rechargeable batteries that are used as the power source for electronic devices. Table 1.1 compares different characteristics of these batteries [1]. As can be seen in the table, Li-ion battery has high energy density, high voltage, long lifetime, low self discharge rate, fast charging time, low toxicity, and a wide operating temperature range. These features make Li-ion battery the best choice among the rechargeable batteries for the energy source of portable electronic devices.

Li-ion batteries have been introduced in the early 1980s and commercialized in 1991 [2]. Although the cost of Li-ion battery is rather high, they are still growing in the market and are expected to continue growing over the next years [3]. Electric

Table 1.1: Comparison between characteristics of four different batteries [1]

Characteristics	Lead-acid	Ni-Cd	Ni-MH	Li-ion
Energy density (Wh/kg)	30-50	40-60	60-120	170-250
Energy density (Wh/L)	60-110	150-190	140-300	350-700
Voltage	2.0	1.2	1.2	3.7
Expected life cycle	300	1500	1000	500-2000
Self-discharge per month (%)	5	20	30	<10
Fast charging time (h)	8-16	1	1-4	1 or less
In use since	Late 1800	1950	1990	1991
Toxicity	High	High	Low	Low
Overcharge tolerance	High	Moderate	Low	Low
Operating temperature range (°C)	-20 to 60	-40 to 60	-20 to 60	-20 to 60

vehicles have the highest demand of Li-ion batteries among others. Fig. 1.1 shows the increasing demand of Li-ion batteries for electric vehicles in the past few years and provides a forecasting of the demands over the next ten years [4]. Also, Fig. 1.2 illustrates the cost prediction of Li-ion battery pack over the next ten years. Although the price of the battery pack is decreasing, its growing demand makes the overall yearly dollar expense in EV industry increasing. Based on Fig. 1.1, 1.2, the overall dollar expense in EV industry will be around \$100 billion per year by the year 2030. This means extending the battery life by 5% will save approximately \$5 billion per year. Moreover, the unexpected events (such as overcharging and overdischarging) that can endanger the life of the batteries can cause billions of dollars' worth of damage. All these reasons urge the need for a monitoring system that prevents unexpected incidents to the battery and prolongs its lifetime. In the next section, battery management systems (BMS) will be introduced to address this problem.

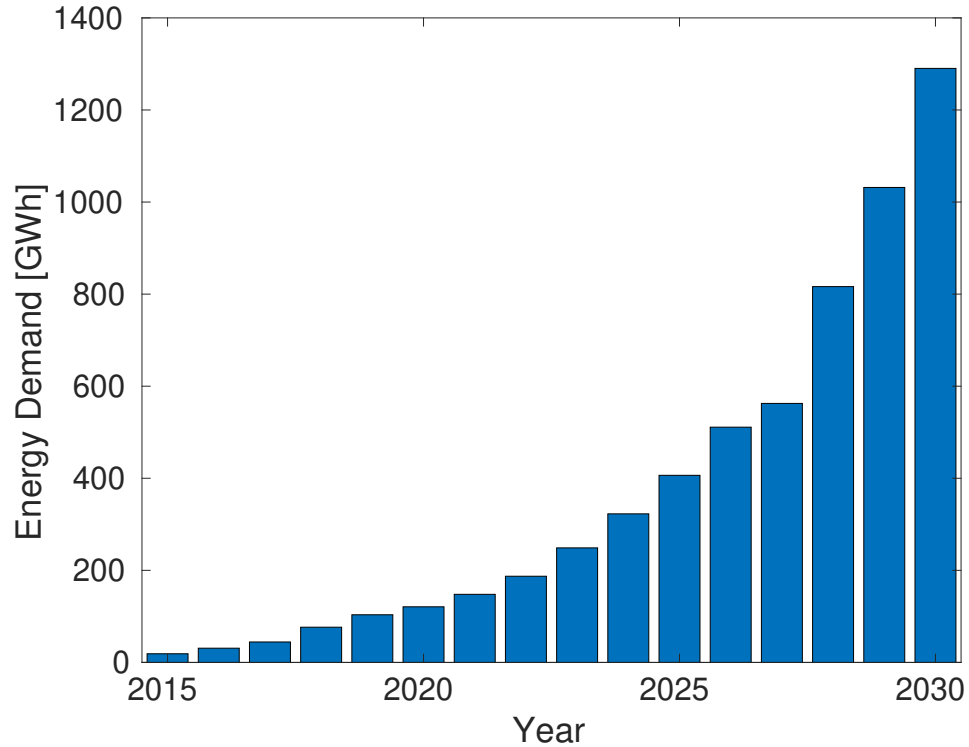


Figure 1.1: Li-ion battery worldwide demand in electric vehicles and prediction for the next ten years [4]

## 1.2 Battery Management Systems (BMS)

As mentioned in the previous section, the high price of Li-ion battery has created the need for monitoring the battery to avoid catastrophic events that will lead to costly expenses. A battery management system (BMS) is employed to monitor the battery and prevent the battery voltage and temperature from exceeding or dropping below certain limits and prevent the overcharging and overdischarging of the battery to ensure its safe and stable operation [7]. Fig. 1.3 depicts the key features of a BMS [8].

In Fig. 1.3, SOC and SOH denote the state of charge and the state of health of the battery, which are indicators of battery charging level and health level respectively. Accurate estimation of SOC and SOH are critical tasks of a BMS, and require special attention. In this thesis, the main objective is to accurately estimate the battery SOC and SOH with low complexity and without interrupting the operation of the battery

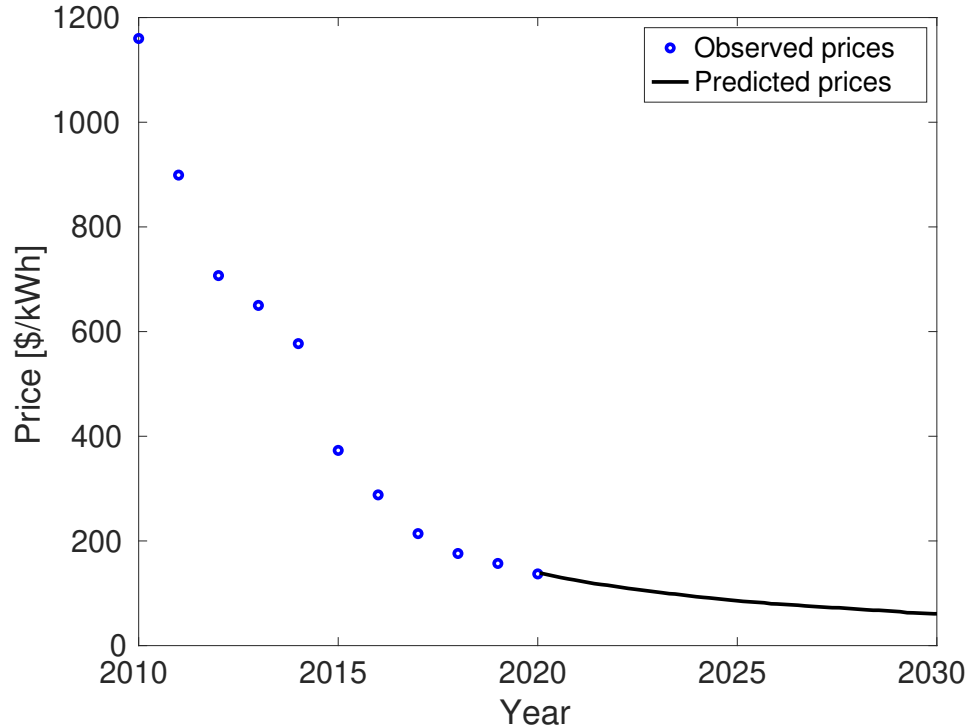


Figure 1.2: Li-ion battery pack cost prediction over the next ten years, based on Bloomberg New Energy Finance (BNEF) forecast [5], [6]

while in use.

### 1.3 Thesis Overview

In this thesis, we propose a novel method with low computational complexity that can accurately estimate the battery SOC and SOH using only partial charge or discharge data and without needing offline tests on the battery. That is, the battery’s SOC and SOH are estimated while the battery is in use and its operation is not interrupted.

In Chapter 2, a background of Li-ion battery modeling will be provided and some of the well known models for Li-ion batteries will be introduced. Also, all the technical terms such as SOC, SOH, DOD, etc. will be defined. Furthermore, Adam optimization algorithm will be briefly introduced and discussed, since it will be used later in the proposed method in chapter 3. Finally, a background on neural networks will be provided. Neural networks are used in Chapter 4.

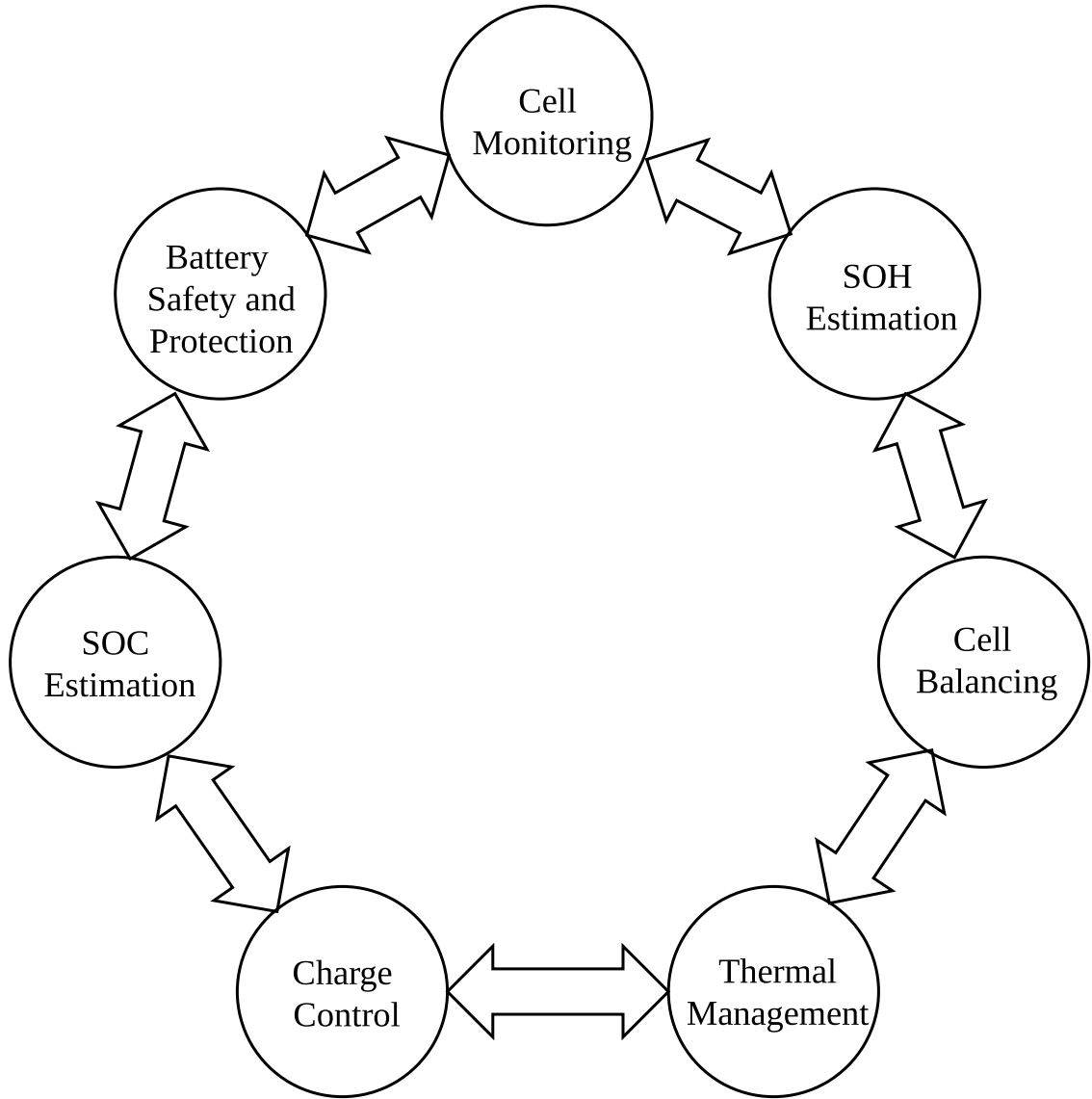


Figure 1.3: BMS key features [8]

In Chapter 3, our novel SOC/SOH estimation method will be explained. In this method, the battery is modeled with a first order equivalent circuit model (ECM) and the parameters of the model are estimated using the measured variables from the last two partial discharge intervals. The estimation of ECM parameters is performed using Adam optimization algorithm, which is a fast gradient based algorithm used to find the optimized parameters for stochastic objective functions [9]. Using the estimated parameters of ECM, the SOH and SOC of the battery will consequently be

estimated. It will be shown that SOH and SOC estimations are obtained extremely fast and the results are highly accurate.

In Chapter 4, the effect of temperature on SOH estimations will be assessed. First, the effect of temperature on the battery internal resistance will be modeled by training a neural network. Then, by removing the effect of internal resistance from the discharge profiles provided in the battery datasheet, the reference curves for different temperatures will be obtained. Finally, the SOH estimation for each discharge interval will be performed using a reference curve for its specific operating temperature. It will be observed that SOH estimations is improved if the effect of temperature is considered in the estimations.

Finally, Chapter 5 will give a summary of the contributions of this thesis and give some insights towards possible future works.

# Chapter 2

## Background

As mentioned in Chapter 1, batteries need to be monitored throughout their operation in order to avoid damages and prolong their usable lifetime. In recent years, there has been significant research progress in this regard. To be able to follow this rich literature, a comprehensive background regarding Li-ion battery state characterization and modeling is required. This chapter provides all the required backgrounds regarding Li-ion battery that the reader will need for Chapters 3, 4. An interested reader who plans to read beyond this thesis is referred to [10]-[13] for a more comprehensive background on Li-ion battery.

The rest of this chapter is as follows. First, battery performance indicators such as SOH, SOC, etc. will be reviewed. Next, different modelings of Li-ion battery will be introduced and discussed. Afterwards, Adam optimization algorithm, which will be used later in Chapter 3, will be briefly explained. Finally, a quick review on neural networks will be provided. Neural networks are used in Chapter 4.

### 2.1 State Characterization for Li-ion Batteries

There are several different ways to characterize the state and performance of batteries. These characterizations will be briefly discussed and explained in this section.

### 2.1.1 State of Charge

SOC is the ratio of the available charge capacity (also called capacity) of the battery ( $Q_{current}$ ) to the capacity of a fully charged battery ( $Q_{FC}$ ) expressed in percentage [14]. That is

$$\text{SOC} = \frac{Q_{current}}{Q_{FC}}. \quad (2.1)$$

SOC is an indication of the available charge in the battery at each moment. In this thesis for simplicity,  $Q_{FC}$  is represented by  $Q$ . If the initial SOC is known, SOC can be estimated from the load current drawn from the battery as [15]:

$$\text{SOC}(t) = \text{SOC}(t_0) - \frac{\int_{t_0}^t \eta I_L(\tau) d\tau}{Q} \quad (2.2)$$

where  $I_L$  is the load current and  $\eta$  is the coulombic efficiency that is defined as the ratio of the charge delivered during discharge and the charge stored during previous recharge [15]. If there are no significant unwanted parasitic reactions in a Li-ion cell and if the electrodes show no significant mechanical degradation, then the coulombic efficiency can be assumed as unity. In this work, we assume  $\eta = 1$ . This assumption is numerically justified in Chapter 3, using available charge-discharge data of Li-ion batteries.

### 2.1.2 State of Health

Electrochemical mechanisms lead to gradual health deterioration of the battery. The capacity fade and internal resistance growth are two consequences of battery aging. SOH is an indicator of the battery health expressed in percentage. There are generally two definitions for the battery SOH, either based on the capacity or the internal resistance. The more common definition of SOH is based on the capacity of the battery [16]:

$$\text{SOH} = \frac{Q}{Q_{rated}}, \quad (2.3)$$

where  $Q$  is the capacity of the fully charged battery at current state and  $Q_{rated}$  is the rated capacity of the unaged battery. The other less common definition of SOH is

based on the internal resistance of the battery [16]:

$$\text{SOH} = \frac{R_{\text{current}} - R_{\text{rated}}}{R_{\text{rated}}}. \quad (2.4)$$

where  $R_{\text{current}}$  is the current internal resistance of the battery and  $R_{\text{rated}}$  is the rated internal resistance of the unaged battery. The first definition (2.3) is used in this study.

A used battery eventually reaches its so-called End-of-Life (EOL), after which its performance will degrade very quickly. According to [16], [17], either a 20%-30% decrease in the battery maximum capacity or a 100% increase in its internal resistance can be considered as the battery EOL.

### 2.1.3 Depth of Discharge

Depth of discharge (DOD) is the ratio of the discharged capacity of the battery ( $Q_{\text{released}}$ ) to the capacity of a fully charged battery ( $Q$ ). In fact, DOD is the complementary of SOC.

$$\text{DOD} = \frac{Q_{\text{released}}}{Q} = 1 - \frac{Q_{\text{current}}}{Q}. \quad (2.5)$$

### 2.1.4 Remaining Useful Life

Battery remaining useful life (RUL) is an indicator of the number of remaining fully charge and discharge cycles that battery is expected to operate. Based on [18], battery RUL is defined as follows:

$$N_{\text{RUL}} = N_{\text{EOL}} - N_{\text{ECL}} \quad (2.6)$$

where  $N_{\text{RUL}}$  is the expected cycle numbers until the battery RUL,  $N_{\text{EOL}}$  is the battery end of life cycle's number, and  $N_{\text{ECL}}$  is the equivalent circle life of the battery.

## 2.2 Li-ion Battery Modeling

There are various equivalent circuit models (ECM) introduced for Li-ion batteries. These models can describe the behaviour of the batteries in terms of physical elements

and therefore can be useful to estimate the battery states, defined in Section 2.1. [19] has categorized the circuit models into five categories, which will be discussed in the following subsections.

### 2.2.1 The $R_{\text{int}}$ Model

The  $R_{\text{int}}$  model is the simplest circuit model for a Li-ion battery, which connects the battery open circuit voltage (OCV) to its terminal voltage  $V_T$  via a series internal resistance  $R_s$  and is shown in Fig. 2.1. Note that  $V_{oc}$  (OCV) and  $R_s$  are both functions of SOC, SOH, and temperature.  $I_L$  is the load current and is positive at discharge and negative at charge. (2.7) shows the equation of the  $R_{\text{int}}$  model.

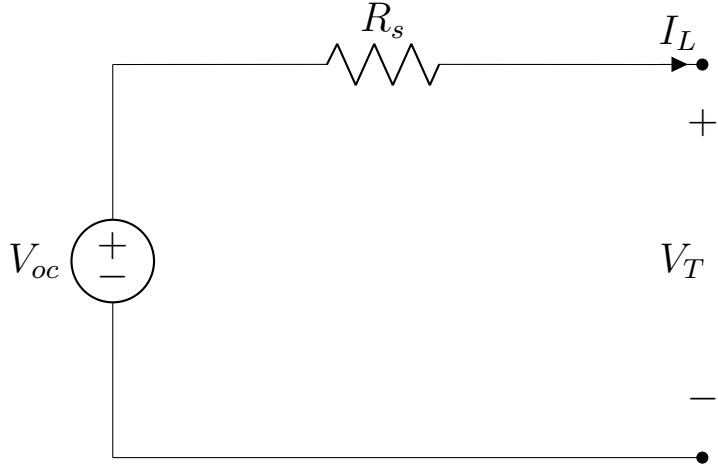


Figure 2.1: Diagram of the  $R_{\text{int}}$  model

$$V_T = V_{oc} - R_s I_L. \quad (2.7)$$

### 2.2.2 The RC Model

The RC model is another circuit model, which was first introduced by the SAFT Battery Company and is illustrated in Fig. 2.2. It can be seen that the model is composed of five elements as follows. The surface capacitor  $C_c$ , the bulk capacitor  $C_b$ , the terminal resistor  $R_t$ , the end resistor  $R_e$ , and the capacitor resistor  $R_c$ . The surface capacitor  $C_c$  has a small capacitance and models the dynamical behaviours of

the battery [20]. The bulk capacitor  $C_b$  has a rather large capacitance and models the charge storing of the battery and can be used to estimate the battery SOC. Equations (2.8) and (2.9) describe the dynamic of the RC model.

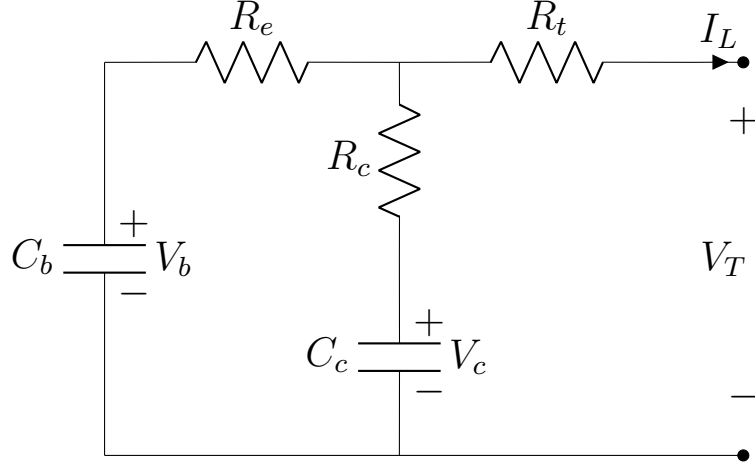


Figure 2.2: Diagram of the RC model

$$\begin{bmatrix} \dot{V}_b \\ \dot{V}_c \end{bmatrix} = \begin{bmatrix} \frac{-1}{C_b(R_e+R_c)} & \frac{1}{C_b(R_e+R_c)} \\ \frac{1}{C_c(R_e+R_c)} & \frac{-1}{C_c(R_e+R_c)} \end{bmatrix} \begin{bmatrix} V_b \\ V_c \end{bmatrix} + \begin{bmatrix} \frac{-R_c}{C_b(R_e+R_c)} \\ \frac{-R_e}{C_c(R_e+R_c)} \end{bmatrix} [I_L], \quad (2.8)$$

$$[V_T] = \begin{bmatrix} \frac{R_c}{R_e+R_c} & \frac{R_e}{R_e+R_c} \end{bmatrix} \begin{bmatrix} V_b \\ V_c \end{bmatrix} + \begin{bmatrix} -R_t - \frac{R_e R_c}{(R_e+R_c)} \end{bmatrix} [I_L]. \quad (2.9)$$

### 2.2.3 The Thevenin Model

The Thevenin model can be considered as an upgraded version of the  $R_{\text{int}}$  model and can be obtained by adding a parallel RC network in series with the internal resistance in the  $R_{\text{int}}$  model, as shown in Fig. 2.3. The parallel RC network contains the polarization resistance  $R_p$  and the polarization capacitance  $C_p$ . The polarization capacitance  $C_p$  describes the transient response of the battery during its operation. The dynamic behaviour of the Thevenin model is expressed in (2.10).

$$\begin{cases} \dot{V}_p = -\frac{V_p}{R_p C_p} - \frac{I_L}{C_p} \\ V_T = V_{oc} + V_p - R_s I_L \end{cases} \quad (2.10)$$

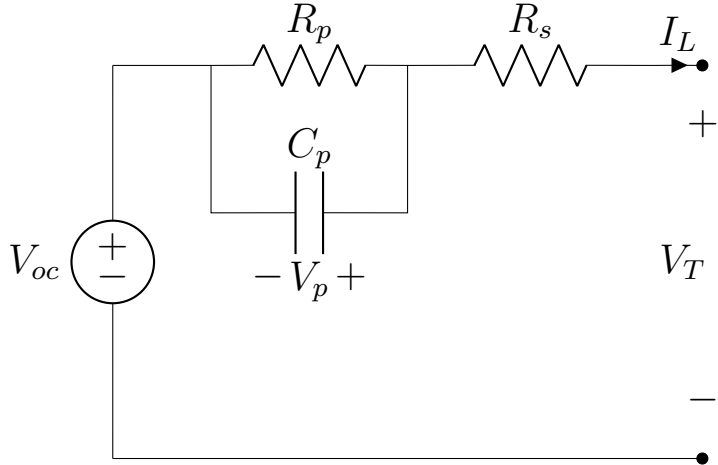


Figure 2.3: Diagram of the Thevenin model

### 2.2.4 The PNGV Model

The PNGV (Partnership for a New Generation of Vehicles) model is an upgrade to the Thevenin model and can be built by adding a capacitor  $\frac{1}{V'_{oc}}$  in series with the internal resistance in the Thevenin model. The capacitor  $\frac{1}{V'_{oc}}$  models the effect of OCV variation with respect to the integral of load current on the terminal voltage [21]. The diagram of the PNGV model is depicted in Fig. 2.4 and the related equations are described in (2.11).

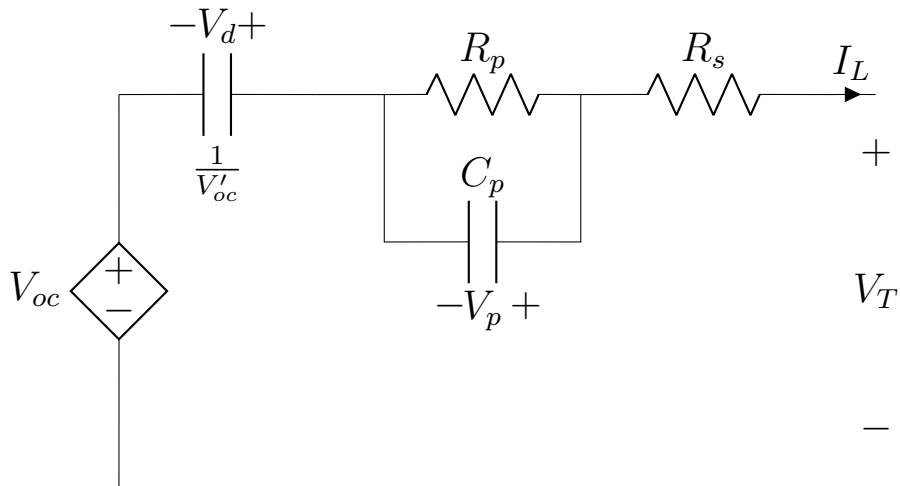


Figure 2.4: Diagram of the PNGV model

$$\begin{cases} \dot{V}_d = -V_o c I_L \\ \dot{V}_p = -\frac{V_p}{R_p C_p} - \frac{I_L}{C_p} \\ V_T = V_{oc} + V_d + V_p - R_s I_L \end{cases} \quad (2.11)$$

### 2.2.5 The DP Model

The dual polarization (DP) model is another upgrade to the Thevinin model and is obtained by adding another parallel RC circuit to the Thevinin model. Based on the provided description of the Thevinin model in Section 2.2.3, the RC network in Fig. 2.3 models the polarization characteristics of Li-ion battery. However, one RC circuit cannot simulate all the polarization characteristics. Therefore, the DP model is used to more accurately simulate the polarization characteristics of the battery. Fig. 2.5 shows the diagram of the DP model and the dynamics of the model are expressed in (2.12).

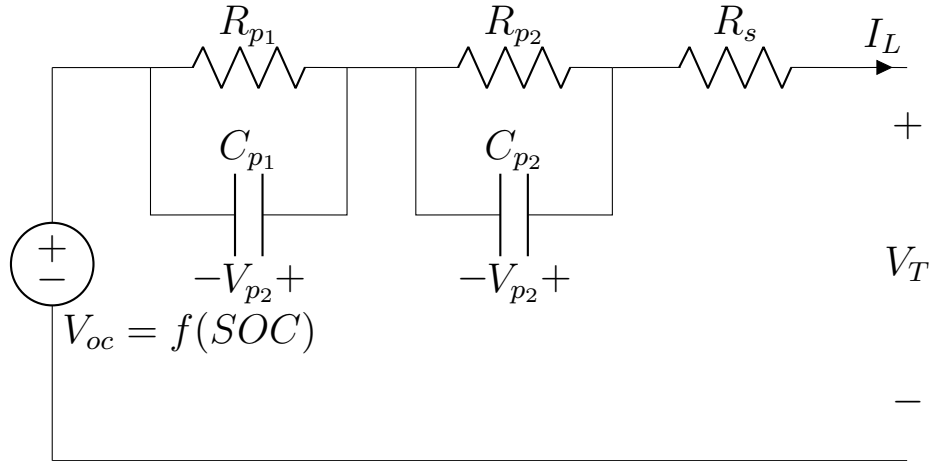


Figure 2.5: Diagram of the DP model

$$\begin{cases} \dot{V}_{p1} = -\frac{V_{p1}}{R_{p1} C_{p1}} - \frac{I_L}{C_{p1}} \\ \dot{V}_{p2} = -\frac{V_{p2}}{R_{p2} C_{p2}} - \frac{I_L}{C_{p2}} \\ V_T = V_{oc} + V_{p1} + V_{p2} - R_s I_L \end{cases} \quad (2.12)$$

## 2.2.6 Higher Order ECMs

In the previous section, five different models for Li-ion battery was introduced. Among them, the Thevinin model and the DP model are used more frequently as Li-ion battery ECM in different studies. The Thevinin model and the DP model are are also called the first and second order ECMs. By adding more RC circuits to these models, higher order ECMs are created. Fig. 2.6 shows the diagram of the  $n^{\text{th}}$  order ECM.

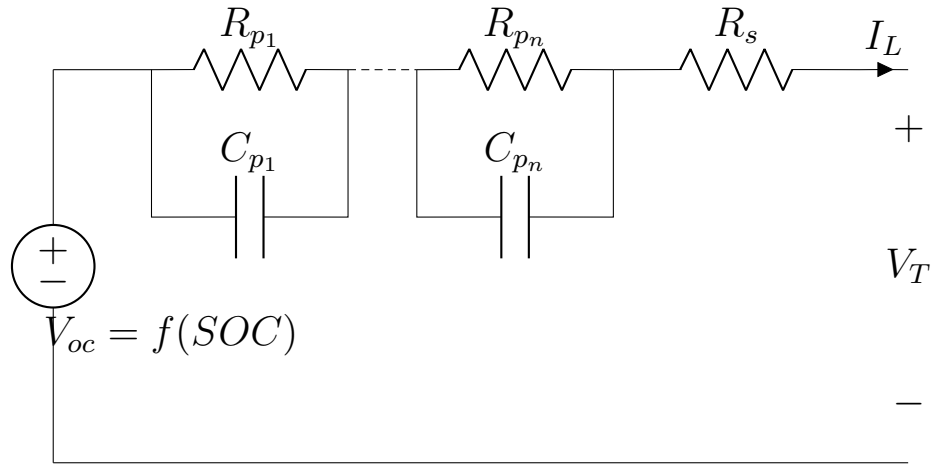


Figure 2.6: Equivalent circuit model of order  $n$  for Li-ion batteries

## 2.2.7 The Selected Model

In this study, the first order ECM (the Thevenin model) is used to model Li-ion battery behaviour. The  $R_{\text{int}}$  model is too simple and cannot describe the behaviour of the battery well. Also, the RC model and PNGV model are not not regarded as the best available models in the literature. Therefore, either a first order or a higher order ECM should be used as the battery model. Although higher order ECMs can potentially model the battery with higher accuracy, they lack generality and may overfit the parameters for a specific battery. As a result, the first order ECM seems to be a good choice.

Fig. 2.7 shows the complete diagram of a first order ECM that shows how the

battery OCV is related to its SOC [22], [23]. In this model,  $V_T$  and  $I_L$  are the terminal voltage and the load current of the battery, where  $I_L$  is considered positive for a discharge and negative for a charge cycle. These two variables can be measured during the battery operation. Using NASA dataset [24], Fig. 2.8 shows  $V_T$  and  $I_L$  for a full discharge interval of an operational battery. Other parameters of the model include the internal resistance  $R_s$ , polarization resistance and polarization capacitance  $R_p$  and  $C_p$ , the polarization voltage  $V_p$  and the open circuit voltage  $V_{oc}$  (OCV) that is a strictly increasing monotonic function of the battery SOC. The SOC-OCV curve for a 18650 Li-ion battery is depicted in Fig. 2.9 [25]. After solving (2.10), the equations of the model at sample  $k$  can be written as follows [26]:

$$V_T[k] = V_{oc}[k] - R_s[k]I_L[k] + V_p[k], \quad (2.13)$$

$$V_p[k] = -R_p I_L[k] + (V_p[k-1] + R_p I_L[k])e^{-\frac{t[k]-t[k-1]}{R_p C_p}}. \quad (2.14)$$

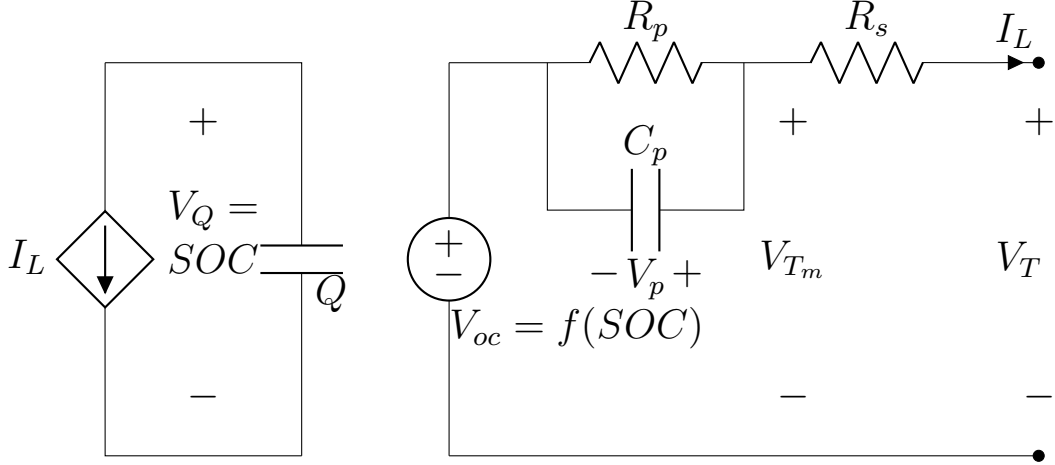


Figure 2.7: First order equivalent circuit model of Li-ion batteries

The relationship between the measurable variables  $V_T$  and  $I_L$  with the rest of the model is given by (2.13) and the dynamic response of the RC circuit is determined by (2.14), where  $k$  represents the sample number. Also  $V_{T_m}$  (modified terminal voltage) is the terminal voltage minus the voltage of internal resistance  $R_s$  that will be further discussed in Section 3.4.2. The left segment of ECM in Fig. 2.7 shows the relationship

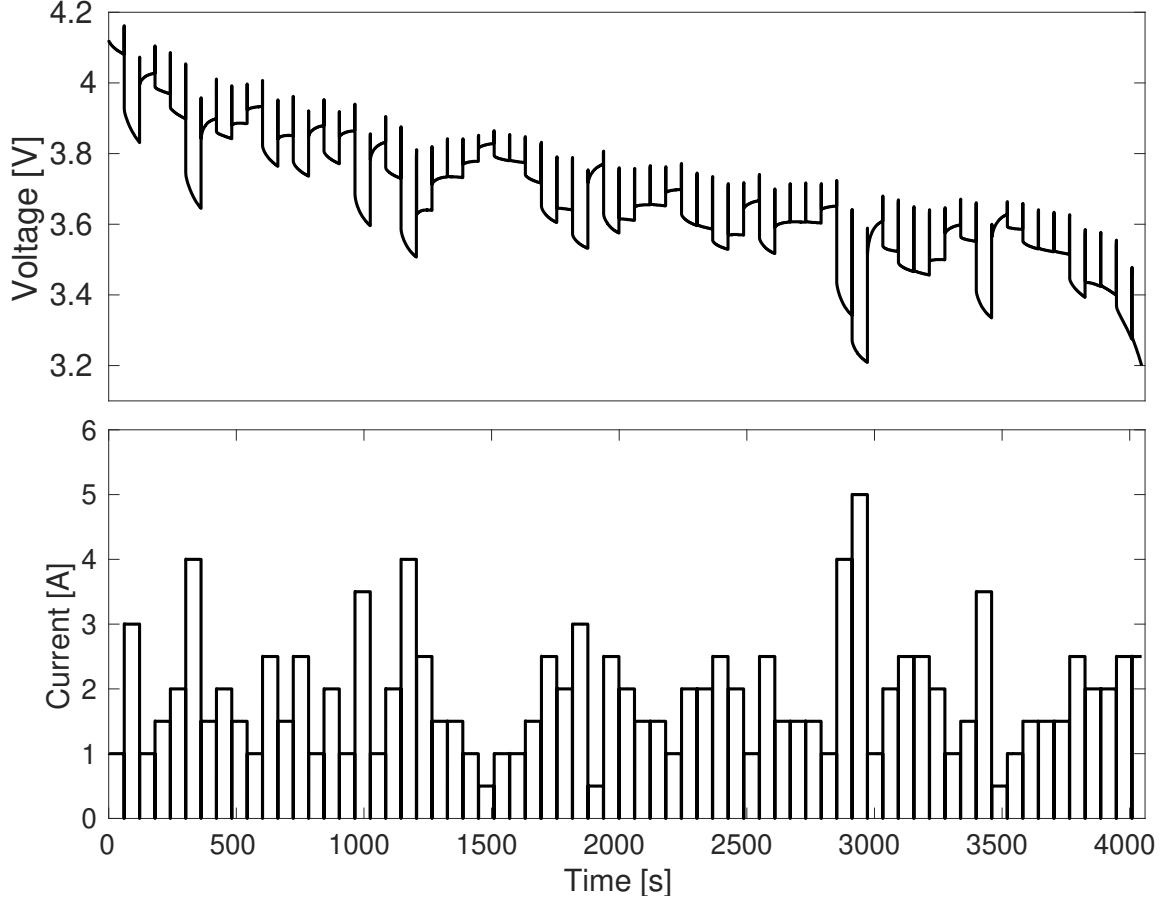


Figure 2.8: A full discharge interval (a) Measured terminal voltage  $V_T$  and (b) Measured load current  $I_L$  profile.

between battery SOC with the cumulative current,  $\int_{t_0}^t I_L(\tau)d\tau$ , which is the physical expression of (2.2).

## 2.3 Adam Optimization Algorithm

Adaptive moment estimation, known as Adam optimization algorithm is a fast gradient based algorithm used to find the optimized parameters for stochastic objective functions. Adam only uses the first order gradients, which requires low memory storage. Table 2.1 shows Adam optimization algorithm step by step. In this algorithm, an stochastic scalar objective function  $f(\theta)$  gets optimized with respect to its parameters  $\theta$ . As can be seen in Table 2.1, the algorithm starts with an initial set of parameters  $\theta_0$  and the parameters update until convergence. The updating process

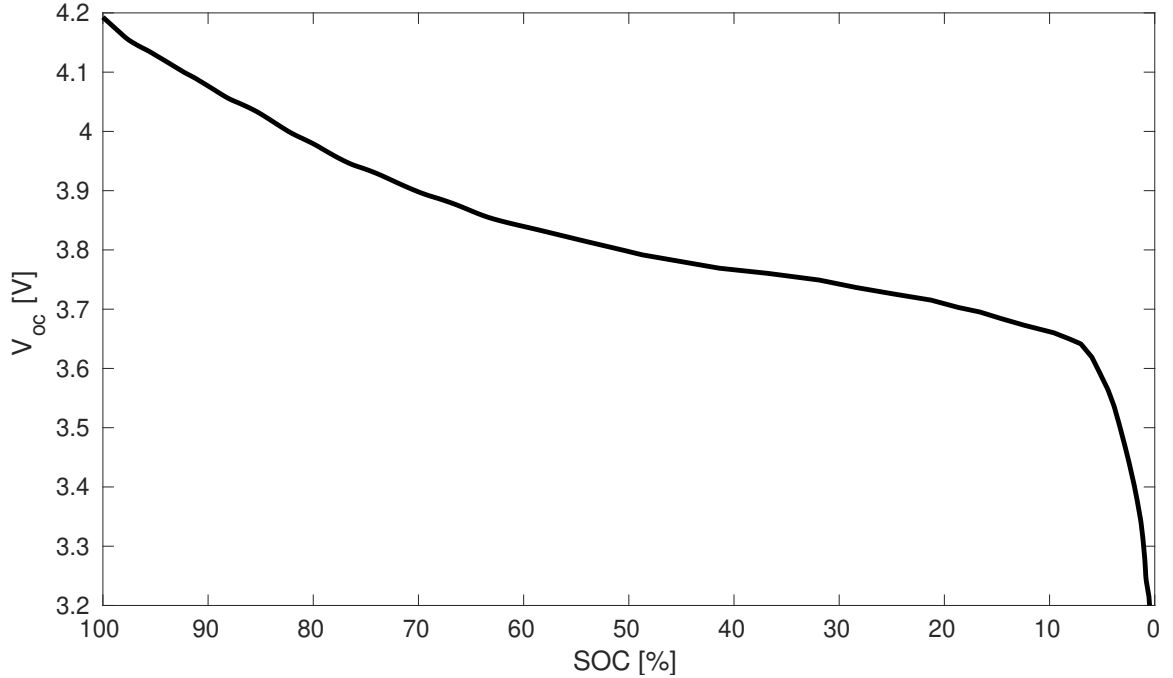


Figure 2.9: SOC-OCV curve for a 18650 Li-ion battery [25]

requires four hyper parameters:  $\alpha$ ,  $\beta_1$ ,  $\beta_2$ , and  $\epsilon$ . These hyper parameters need to be tuned beforehand. The parameters  $\alpha = 0.001$ ,  $\beta_1 = 0.9$ ,  $\beta_2 = 0.999$  and  $\epsilon = 10^{-8}$  are tuned on some known datasets and seem to work well as the default settings for most problems [9].

Adam will be used as the optimization algorithm in this study, because of its many advantages and superiority in terms of convergence time, memory usage, and complexity compared to other optimization algorithms.

## 2.4 Neural Networks

An artificial neural network (NN) is a series of connected units called neurons, sorted layer by layer, each passing information along to their next layer, as illustrated in Fig. 2.10. Each neuron performs a mathematical function on the information it receives from its previous layer and passes the result to the next layer. This function is called the activation function. The first layer of a neural network is called the input layer and the last layer is called the output layer. All the layers between the input and the

Table 2.1: Adam optimization algorithm:  $g_t^2$  indicates the element-wise square  $g_t \odot g_t$ . Good default settings for the tested machine learning problems are  $\alpha = 0.001, \beta_1 = 0.9, \beta_2 = 0.999$  and  $\epsilon = 10^{-8}$ . All operations on vectors are element-wise [9].

---



---

**Require:**  $\alpha$ : Stepsize

**Require:**  $\beta_1, \beta_2 \in [0, 1)$ : Exponential decay rates for the moment estimates

**Require:**  $f(\theta)$ : Stochastic objective function with parameters  $\theta$

**Require:**  $\theta_0$ : Initial parameter vector

$m_0 \leftarrow 0$  (Initialize first moment vector)

$v_0 \leftarrow 0$  (Initialize second moment vector)

$t \leftarrow 0$  (Initialize timestep)

**while**  $\theta_t$  not converged **do**

$t \leftarrow t + 1$

$g_t \leftarrow \nabla_{\theta} f_t(\theta_{t-1})$  (Get gradients w.r.t. stochastic objective at timestep  $t$ )

$m_t \leftarrow \beta_1 \cdot m_{t-1} + (1 - \beta_1) \cdot g_t$  (Update biased first moment estimate)

$v_t \leftarrow \beta_2 \cdot v_{t-1} + (1 - \beta_2) \cdot g_t^2$  (Update biased second raw moment estimate)

$\hat{m}_t \leftarrow m_t / (1 - \beta_1^t)$  (Compute bias-corrected first moment estimate)

$\hat{v}_t \leftarrow v_t / (1 - \beta_2^t)$  (Compute bias-corrected second raw moment estimate)

$\theta_t \leftarrow \theta_{t-1} - \alpha \cdot \hat{m}_t / (\sqrt{\hat{v}_t} + \epsilon)$  (Update parameters)

**end while**

**return:**  $\theta_t$ : (Resulting parameters)

---



---

output layer are called the hidden layers. In the example of Fig. 2.10, the input layer has three neurons or nodes and the output layer has one neuron. There are also two hidden layers with ten and three neurons respectively [27], [28].

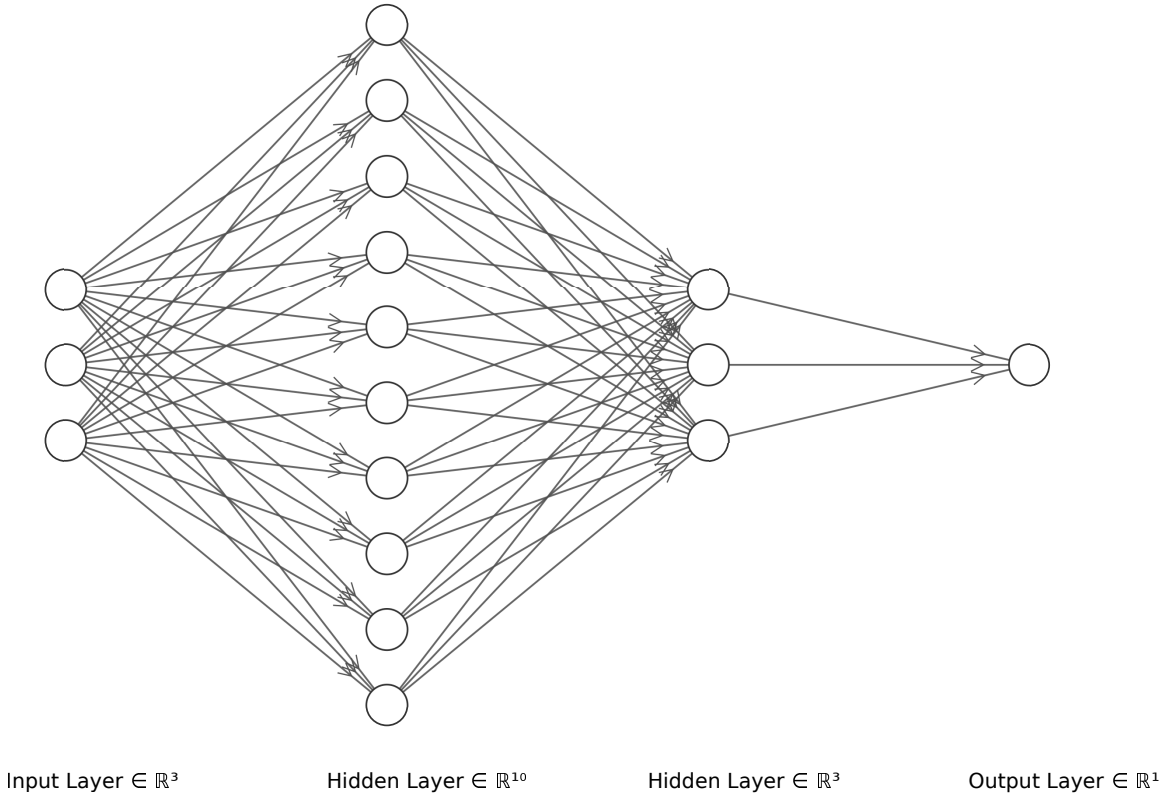


Figure 2.10: A fully connected neural network with three inputs, one output and two hidden layers with ten and three neurons respectively

As can be seen in Fig. 2.10, the neurons of each layer are connected to the neurons of their next layer. Each connection has a weight  $w$ . If  $n$  inputs  $x_1, x_2, \dots, x_n$  with the respective weights  $w_1, w_2, \dots, w_n$  get passed into a neuron with the activation function  $f$ , the output of that neuron is given by:

$$O = f(net) = f\left(\sum_{j=1}^n w_j x_j\right), \quad (2.15)$$

in which  $net$  is the weighted input of the neuron and is obtained by the dot product of the input vector and the weight vector:

$$net = w^T x = w_1 x_1 + \dots + w_n x_n, \quad (2.16)$$

where  $T$  denotes the matrix transpose operation. The activation function  $f$  can be any mathematical function. The simplest activation function using in neural networks is:

$$O = f(net) = \begin{cases} 1 & \text{if } w^T x > 0 \\ 0 & \text{otherwise} \end{cases} \quad (2.17)$$

where  $\theta$  is the threshold level of that neuron. A neuron with this type of activation function is called a linear threshold unit.

There are other commonly used activation functions, including sigmoid, tanh, relu, etc. The formula of these activation functions are expressed in equations (2.18)-(2.20).

Sigmoid:

$$O = f(net) = \frac{1}{1 + e^{-net}}, \quad (2.18)$$

Tanh:

$$O = f(net) = \frac{2}{1 + e^{-net}} - 1, \quad (2.19)$$

Relu:

$$O = f(net) = \max(0, net). \quad (2.20)$$

There are lots of other activation functions used in neural networks as well, but the above three activation functions are the most common used.

### 2.4.1 Neural Networks Training

A neural network is one of the most powerful tools used to find the complex relationships between some inputs and their related outputs. A large set of training data is needed to train the network weights properly, so that the predicted outputs would match their true values with minimum error. An optimization algorithm is used to train the weights. After training the network, by giving some inputs to the network, it can predict their output based on the trained weights. When the relationship between the inputs and the outputs is unknown, a neural network is a very useful tool. In Chapter 4, neural networks will be used to find the relationship between the inputs temperature, SOC, and SOH and the output internal resistance of the battery.

# Chapter 3

## The Proposed Method

### 3.1 Introduction

Various battery state estimation methods are reported in the literature that can be classified into offline, online with offline training, and fully online methods. Offline methods such as enhanced coulomb counting [29], open circuit voltage method [30], and impedance spectroscopy [31, 32] need the battery voltage, current or temperature data acquired under certain test conditions offline, interrupting the battery's normal operation. Hence, offline methods are not practical in many applications. Offline methods, however, provide an accurate estimation of the battery's capacity and SOH, which can be used as reference values for validating other types of estimations.

A number of other methods are also proposed that use offline training while performing battery state estimations based on online measurements. These works use techniques such as artificial neural networks (ANN) [33], support vector machines (SVM) [34], long short term memory neural networks (LSTM) [35], [36], extreme learning machines (ELM) [37], [38], and the incremental voltage difference based technique [39]. These methods consider the battery as a black box and use a large set of training data to train a SOH estimation algorithm. These trained algorithms normally provide accurate results on the test data and provide highly accurate estimations of SOH. The main limitation of such hybrid methods is that they need sufficient valid data for training and this data may not be readily available for all

types of Li-ion batteries and applications.

The third category is fully online methods that do not need any kind of offline measurement or training. Examples are incremental capacity analysis (ICA) [40], [41], [42], and differential voltage analysis (DVA) [43], [44] that use geometric features of battery data such as peaks in the first derivative of charging curves, to estimate SOH. These methods are very easy to implement and have low complexity. However, they require the battery to pass through some specific SOC ranges, which might not always happen in practice. Adaptive methods that use equivalent circuit model (ECM) to emulate battery behaviour have also been widely used. Recursive least square (RLS) [45]-[47] and extended Kalman filter [48], [49] are some of the methods used to estimate the parameters of ECM. These adaptive methods are completely online and do not need the battery to pass through specific points. Some of the drawbacks include a relatively long convergence time and strong dependency on the initial points in the estimations.

## 3.2 Problem Definition

The main goal in this study is to estimate the battery SOH based on partial discharge data and without circuit interruption. As  $Q_{rated}$  is provided by datasheets, the estimation of SOH is equivalent to the estimation of  $Q$ , according to (2.3).

Based on (2.2), if a battery gets discharged with a low current from 100% SOC (fully charged state) to 0% SOC (fully discharged state),  $Q$  can be computed by:

$$Q = \int_{T_{FD}} I_L(\tau) d\tau \quad (3.1)$$

where  $T_{FD}$  represents a complete discharge period. As mentioned in Chapter 2, it is assumed  $\eta = 1$ , verified as follows. For different aging levels, the integral of the current when the battery was being discharged from the fully charge state was calculated. After the discharge was ended, the integral of the current was again calculated during charging until it was fully discharged. The values of these two integrals were then

divided by each other and the ratio  $\eta$  was observed to be very close to 1 for all aging levels.

This method of calculating  $Q$  is called coulomb counting. When a battery is connected to a load, the measurement of the battery capacity  $Q$  via coulomb counting is impractical, as it requires a full discharge cycle which rarely happens in practice. Therefore, estimating  $Q$  using only partial discharge or charge data is a major challenge that must be resolved for online SOH/SOC estimations.

A partial discharge interval is defined as the time interval between two consecutive charging of the battery. The parameters of each partial discharge interval are demonstrated in terms of the cumulative current,  $\int_{t_0}^t I_L(\tau)d\tau$ , which is called "ISUM" in this thesis. When the battery is in operation, the terminal voltage  $V_T$  and load current  $I_L$  can be accessed without interrupting the battery's operation. Therefore, ISUM is accessible and all parameters can be expressed in terms of ISUM.

To estimate  $Q$  using  $I_L$  and  $V_T$  measurements, circuit model parameters  $R_p$ ,  $C_p$ , and  $R_s$  as well as the relationship between SOC and OCV ( $f(\text{SOC})$ ), as illustrated in Fig. 2.9 should be determined. Initially,  $R_s$  is estimated based on the voltage jumps. Then, based on the assumption that ISUM-OCV is constant for consecutive cycles,  $R_p$  and  $C_p$  are estimated. Based on the estimated parameters, ISUM-OCV will be known and subsequently,  $Q$  can be estimated. The estimation of  $Q$  is based on the assumption that SOC-OCV curve does not change over the life time of a battery. Therefore, by replacing ISUM with  $\text{SOC} = \frac{\text{ISUM}}{Q}$  in ISUM-OCV curve, the correct  $Q$  can be found that results in a close SOC-OCV curve compared to the rated curve. The rated SOC-OCV curve can be extracted from the battery datasheet or the first two discharge cycles of the battery, if available. The assumptions and the details of the proposed method is provided in the next sections.

### 3.3 Basic Ideas and Assumptions

Based on the previous section, the primary goal in this thesis is estimating battery SOC and SOH or interchangeably, battery capacity,  $Q$ . To achieve this goal, battery OCV needs to be estimated using the available measured variables from the partial discharge data. Before discussing the details of the proposed method, two main assumptions are reviewed.

#### 3.3.1 $Q$ Variation is negligible in two consecutive intervals

The full charging capacity of a battery,  $Q$ , varies in a very slow pace during the battery lifespan as the battery aging takes several months. Therefore, it is reasonable to assume that for two consecutive discharge intervals, taking place during a few hours time window,  $Q$  is constant. Therefore, for two consecutive discharge intervals starting with equal SOCs, the OCV curves with respect to ISUM are the same.

#### 3.3.2 Normalized SOC-OCV does not change over the lifetime

Based on [50]-[52], the variation of the relationship between OCV and SOC is negligible at different aging levels in similar temperatures. Suppose at two aging levels  $L_1$  and  $L_2$  with the same temperature, the capacity of the battery is  $Q_1$  and  $Q_2$  respectively. The ISUM-OCV curves for these two aging stages are different, but after normalizing ISUM by  $Q_1$  at level  $L_1$  and by  $Q_2$  at level  $L_2$  using (2.2), the resulting SOC-OCV curves would be the same.

An overview of the proposed solutions is given in here. A more detailed version is given in the next section. To estimate SOH, battery  $Q$  needs to be estimated and to estimate  $Q$ , ISUM-OCV curve is needed. For that, battery ECM is used to model the battery and estimate its parameters, which include OCV as well. The block diagram of the proposed method is shown in Fig. 3.1-3.3 and will be discussed in the next section.

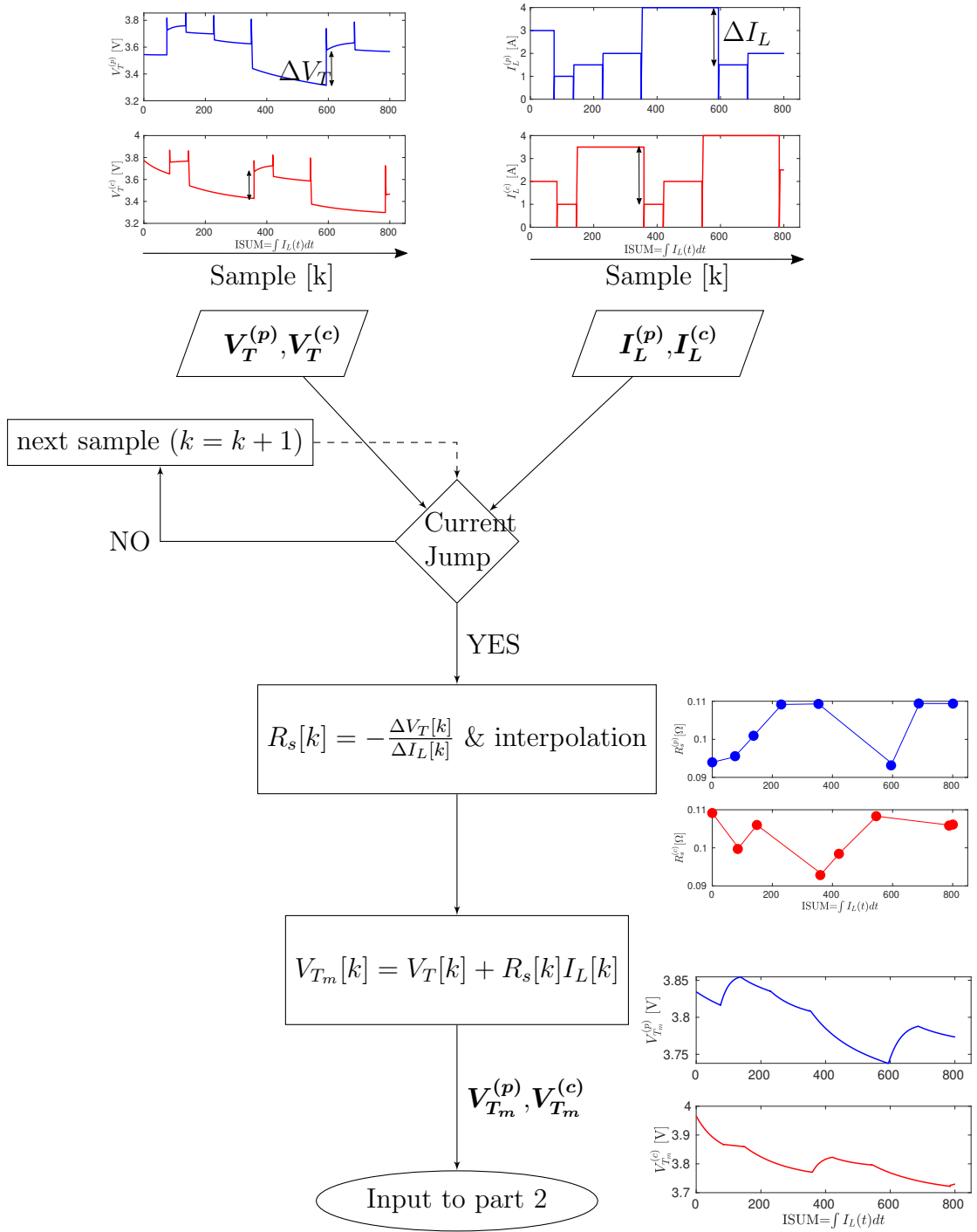


Figure 3.1: Flowchart of the proposed algorithm part 1

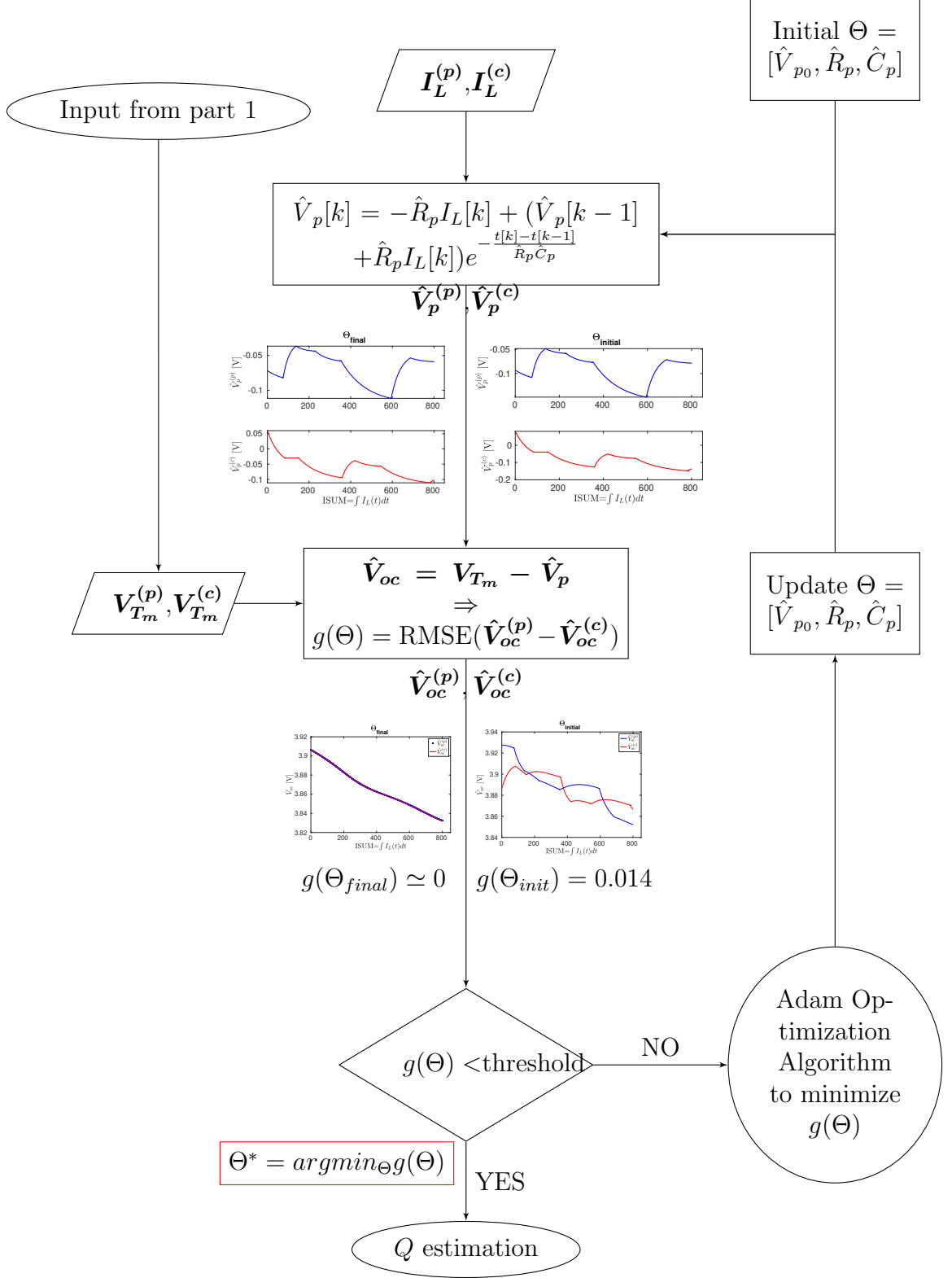


Figure 3.2: Flowchart of the proposed algorithm part 2

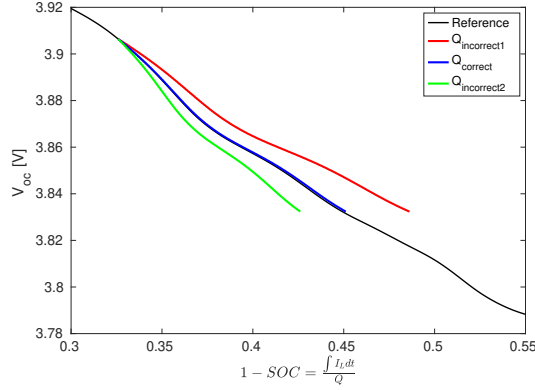
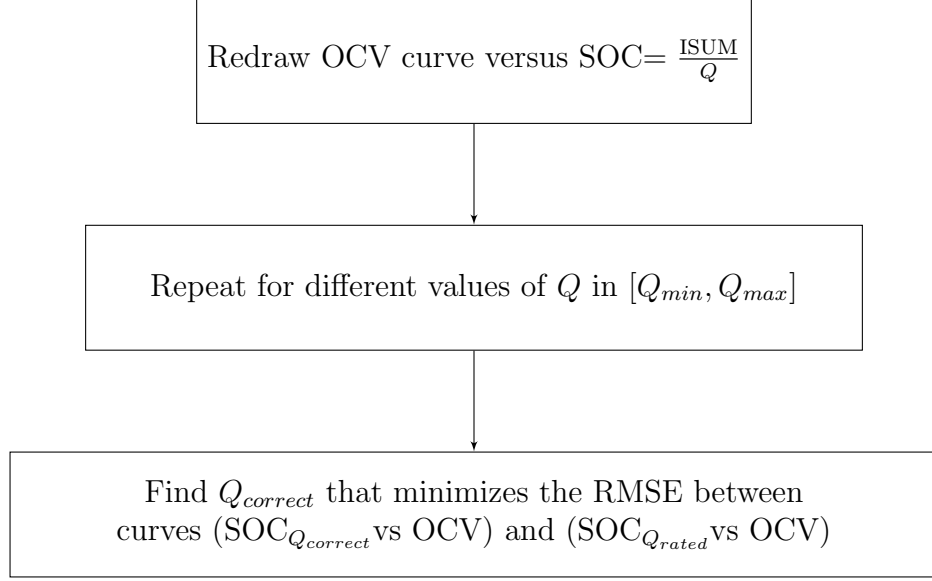


Figure 3.3: Flowchart of the proposed algorithm part 3

## 3.4 Details of the Proposed Method

The proposed method is performed in four consecutive main steps. These steps are discussed one-by-one in the following.

### 3.4.1 Partial Discharge Data Extraction

Here, first the details of the discharge intervals in the NASA dataset [24] will be explained and it will be shown that most of the intervals are partial and therefore are suitable for this study. Then it will be explained how the discharge intervals get extracted from the continuous signals containing repetitive charge and discharge

intervals.

NASA degradation dataset consists of repetitive charge and discharge intervals. The batteries were repeatedly charged to 4.2V and discharged to 3.2V with random currents between 0.5-5 Ampere, that is called random walk (RW) discharging. Although the range 3.2V to 4.2V seems like a full charge/discharge operation, one should note that these voltages refer to the terminal voltage  $V_T$  and not the open circuit voltage  $V_{oc}$ . Fig. 3.4 shows the 156th discharge cycle of B13 in NASA dataset. As can be seen, although the terminal voltage has reached its lower limit (3.2V), the open circuit voltage is about 3.85V which is equivalent to 60% SOC based on Fig. 2.9. More importantly, it should be noted that the proposed method does not use  $V_T$  directly and it operates on the internal voltage  $V_{T_m}$  that is obtained by  $R_s$  from the terminal voltage, as illustrated in Fig. 3.4. This modified terminal voltage only changes in a limited range during each cycle, emulating a partial charge and discharge data. As the proposed method accurately predicts SOH and SOC for such partial data, it can be concluded that it does not require full range data and can achieve similar results for other charge or discharge patterns.

The proposed approach, requires to separate two similar charge or discharge SOC starting points in two consecutive cycles which can be done as shown in Fig. 3.5. Therefore, the signals in the two intervals can be extracted from the original signal and will be called  $\mathbf{V}_T^{(p)}$ ,  $\mathbf{V}_T^{(c)}$ ,  $\mathbf{I}_L^{(p)}$ , and  $\mathbf{I}_L^{(c)}$ , where superscripts  $(p)$  and  $(c)$  represent the previous and current discharge intervals. Note that the way  $\mathbf{V}_T^{(p)}$ ,  $\mathbf{V}_T^{(c)}$  were constructed ensured same ISUM and therefore SOCs.

### 3.4.2 $R_s$ Estimation

Based on (2.13), a step change or discontinuity in  $I_L$  results in a step change or discontinuity in the voltage across the internal resistance  $R_s$ . OCV and  $V_p$  are continuous functions and change smoothly over time. Therefore, any discontinuity in the terminal voltage is caused by  $R_s I_L$ , which is caused by a discontinuity in  $I_L$ . By

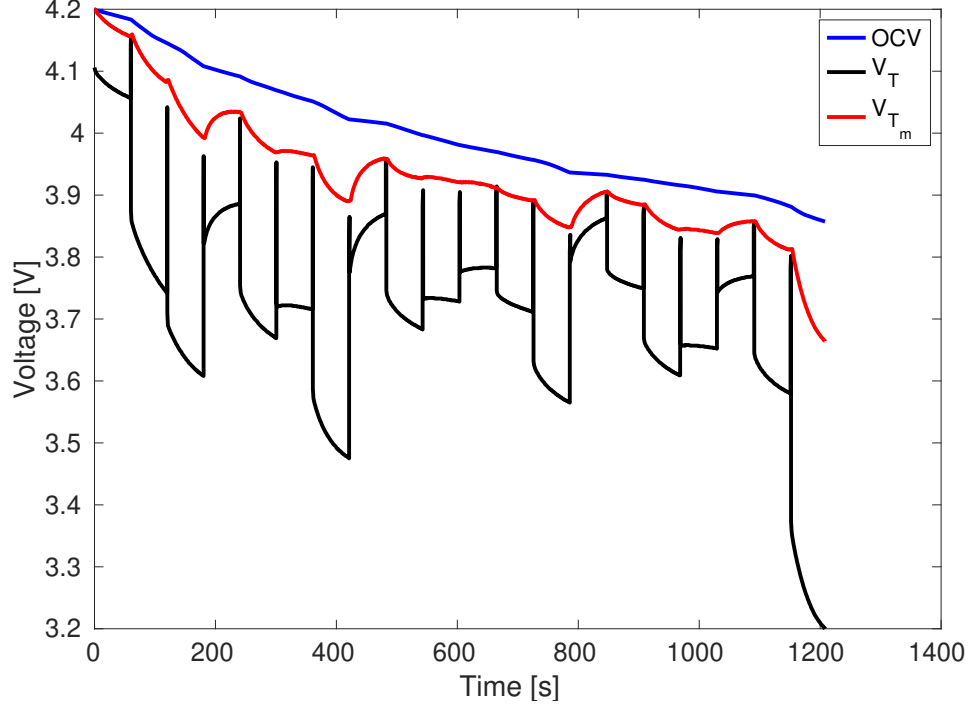


Figure 3.4: terminal voltage versus open circuit voltage in a discharge cycle.

capturing the values of  $\Delta V_T$  and  $\Delta I_L$  at the moments of discontinuity, the internal resistance  $R_s$  can be estimated as:

$$R_s[k] = -\frac{\Delta V_T[k]}{\Delta I_L[k]}, \quad (3.2)$$

where  $k$  is the sample where discontinuity happens.

There might be some oscillations at the instant of step change caused by parasitic components in the power circuit and such oscillations might be sampled by the measurement sensors causing errors. To avoid this, sample  $k+\delta$  is used as the sample after discontinuity to calculate  $\Delta V_T[k] = V_T[k+\delta] - V_T[k]$  and  $\Delta I_L[k] = I_L[k+\delta] - I_L[k]$ , where  $\delta$  is a delay for proper measurements.

The  $R_s$  estimation according to 2.14 is based on the assumption that the samples at time  $k$  and  $k+\delta$  are close enough so that voltage  $V_p$  has not changed significantly. In other words, the time constant should satisfy the following:

$$R_p C_p \geq n(t[k+\delta] - t[k]), \quad (3.3)$$

$$|I_L[k+\delta] - I_L[k]| \geq \xi, \quad (3.4)$$

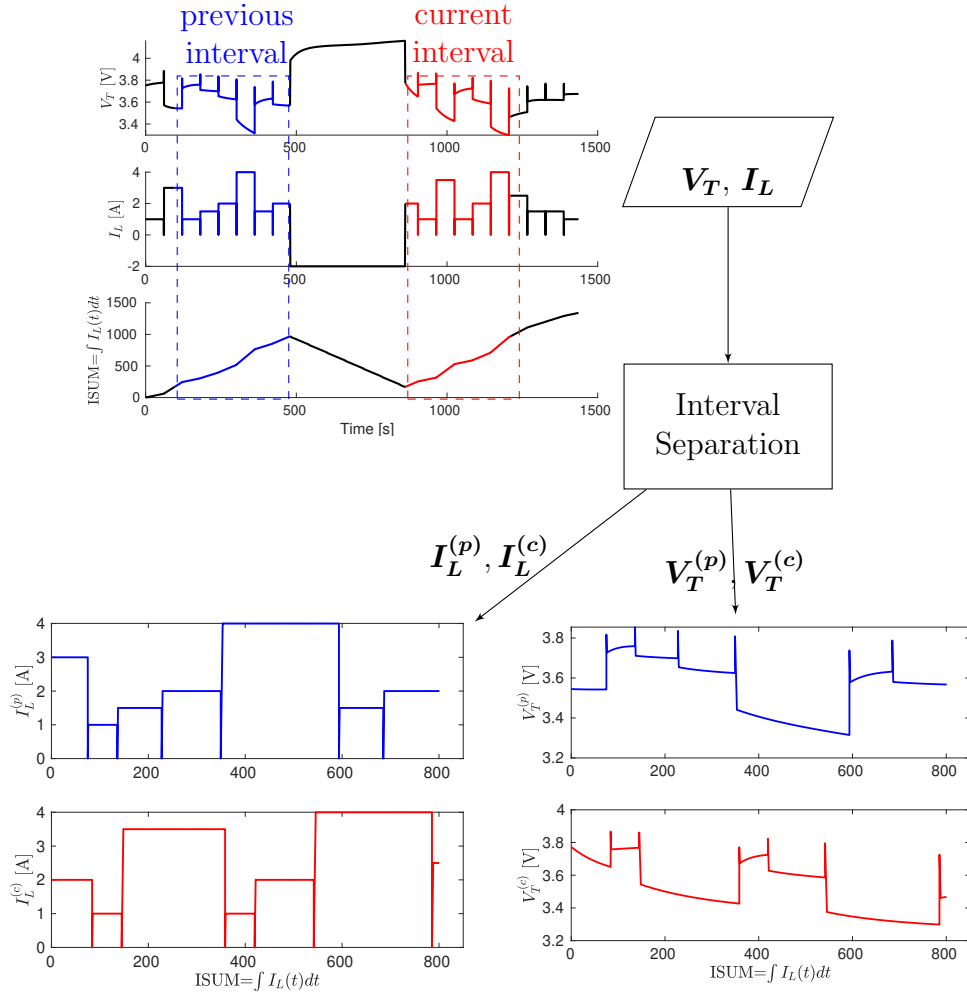


Figure 3.5: Interval separation process: converting the raw signal into the desirable inputs.

where  $n = 10$  and  $\xi = 0.3$  are used in this thesis. In other words, the rate of change of  $V_p$  is 9 times slower than  $R_s I_L$ , thus it is safe to assume that  $\Delta V_T[k]$  is almost completely affected by  $R_s \Delta I_L[k]$  and not  $V_p$ . To consider a current change as a step change,  $\Delta I_L$  should jump higher than  $\xi$  as stated in (3.4), which is considered 0.3 in this study. If a discontinuity does not satisfy conditions (3.3) and (3.4), the estimated  $R_s$  will not be accurate. It is worth mentioning that at least one jump happens in every cycle when the battery switches from discharge to charge and vice versa. Therefore, whenever there is a jump in current,  $R_s$  can be estimated using

(3.2). Based on estimated  $R_s$ , continuous internal voltage,  $V_{T_m}$ , can be estimated as:

$$V_{T_m}[k] = V_T[k] + R_s[k]I_L[k] = V_{oc}[k] + V_p[k]. \quad (3.5)$$

It can be seen in Fig. 2.7 that  $V_{T_m}$  is the voltage seen from the terminal, assuming there is no internal resistance  $R_s$ .

### 3.4.3 $R_p$ , $C_p$ and OCV Estimation

Using the calculated  $V_{T_m}$ , the remaining unknown parameters in the ECM can be estimated. Based on (3.5),  $V_{T_m}$  signal comprised of two signals  $V_{oc}$  and  $V_p$ . As current  $I_L$  is known, assuming an initial value for  $R_p$ ,  $C_p$ , and  $V_{p0}$ ,  $V_p$  can be estimated for the rest of the interval using ECM and (2.14). As  $V_{oc}$  is not known, more information is needed to confirm that the initial values of  $V_{p0}$ ,  $R_p$ , and  $C_p$  were accurate. To overcome this problem, this thesis assumes ISUM-OCV curves are equal for two consecutive discharge cycles. The detailed procedure is as follows. Starting with an initial  $\Theta = [\hat{V}_{p0}, \hat{R}_p, \hat{C}_p]$ , based on (2.14),  $V_p$  for the previous and current intervals,  $\hat{\mathbf{V}}_p^{(p)}$  and  $\hat{\mathbf{V}}_p^{(e)}$  can be calculated. Using the estimated  $\mathbf{V}_{T_m}^{(p)}$  and  $\mathbf{V}_{T_m}^{(e)}$ ,  $\hat{\mathbf{V}}_{oc}^{(p)}$  and  $\hat{\mathbf{V}}_{oc}^{(e)}$  can be calculated. Based on assumption 1, if the estimated  $\Theta$  is the correct set,  $g(\Theta)$ , which is defined in (3.6) should be very small:

$$g(\Theta) = \text{RMSE}(\hat{\mathbf{V}}_{oc}^{(p)} - \hat{\mathbf{V}}_{oc}^{(e)}). \quad (3.6)$$

If the error is not within the specified range, the state of the art optimization algorithm, Adam [9] that is a fast gradient-based optimization method is used to find another set of parameters, and this cycle repeats until for  $\Theta_{final}$ ,  $\hat{\mathbf{V}}_{oc}^{(p)}$  and  $\hat{\mathbf{V}}_{oc}^{(e)}$  are close enough. The final set of estimated parameters give the minimum value for the objective function as shown in (3.7):

$$\Theta^* = \underset{\Theta}{\text{argmin}} g(\Theta). \quad (3.7)$$

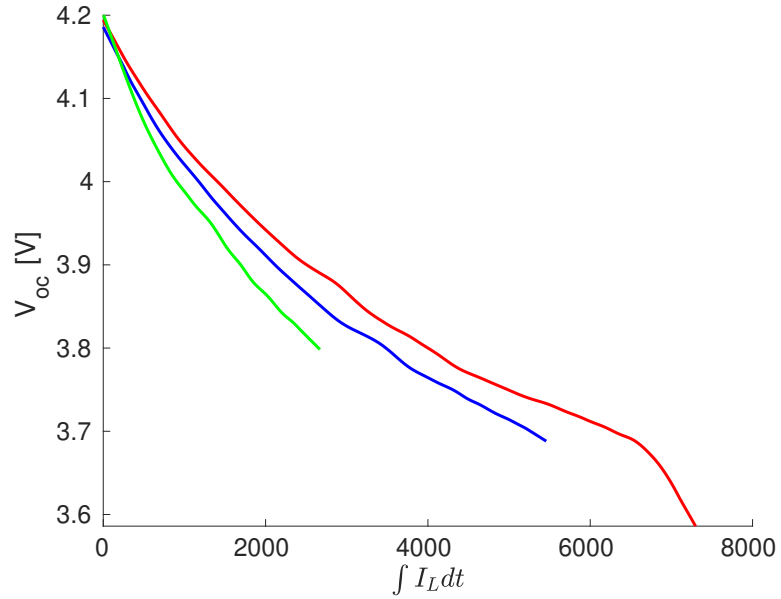
### 3.4.4 SOC-OCV curve and SOH Estimation

Based on the estimated OCV in Section 3.4.3 and constructing ISUM-OCV curve, the capacity  $Q$  and consequently SOH will be estimated in this section. Based on (2.2), ISUM can be normalized to SOC and therefore, the correct value of  $Q$  can normalize ISUM-OCV curve to SOC-OCV curve. According to assumption 2, SOC-OCV curve doesn't change over the battery lifetime. For a brand new battery, it is assumed that SOH=100% and an  $\text{SOC}^{(ref)}$ -OCV curve should be estimated and then as the battery ages, this reference curve will be used to estimate  $Q$  and SOH. Assuming that at the beginning, the maximum electric charge capacity,  $Q = Q_{rated}$ , by normalizing the obtained first cycle's ISUM-OCV curve from Section 3.4.3 by  $Q_{rated}$ , the  $\text{SOC}^{(ref)} - \text{OCV}$  curve will be achieved. Based on  $\text{SOC}^{(ref)} - \text{OCV}$ , the unknown parameter  $Q$  will be swept and for each value, ISUM-OCV will be normalized to obtain corresponding  $\text{SOC}_Q - \text{OCV}$  curve. The value that provides minimum mean square error between the current  $\text{SOC}_Q - \text{OCV}$  and the reference  $\text{SOC}^{(ref)} - \text{OCV}$  is the final estimated value for  $Q$  in that interval. In Fig. 3.6, ISUM-OCV curves and their normalized SOC-OCV curves for three different aging levels are drawn and compared to the reference curve. Using this estimated maximum electric charge capacity  $Q$ , SOH can be obtained using (2.3).

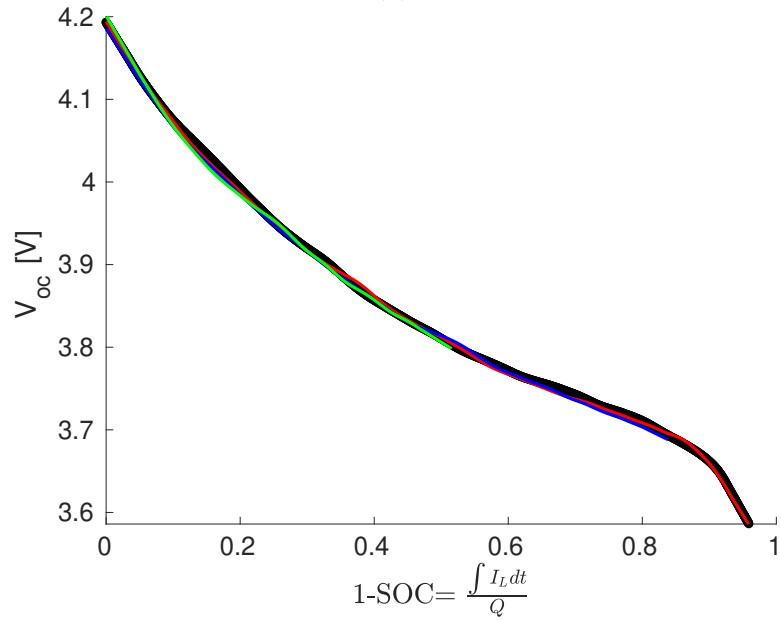
## 3.5 Performance Evaluation

### 3.5.1 Datasets and Verification Method

NASA degradation datasets for Li-ion batteries [24] is used in this work to validate the proposed method. The details regarding the charging and discharging of the batteries in NASA dataset are explained in Section 3.4.1. Fig. 2.8 shows an example of the random walk current in the dataset. This dataset includes seven sets of four 18650 Li-ion batteries, each group being discharge by different distribution of random currents. In this thesis, we applied the proposed method to eight of these batteries



(a)



(b)

Figure 3.6: (a) ISUM-OCV curves at three different aging levels. (b) SOC-OCV curves derived with normalizing ISUM-OCV curves by proper  $Q$  at each aging level and reference SOC-OCV curve (black curve).

(B3, B13, B14, B15, B16, B21, B22, and B23).

After every 50 cycles of charge and discharge, a series of offline reference tests have been applied to measure battery's real capacity. In this study, these measurements are used for the proposed method validation. For these reference tests, the batteries

are first charged using a constant current - constant voltage (CC-CV) charging mode, so that their SOCs reach 100%. Then, they are discharged using a constant 1A current until the terminal voltage reaches 3.2V. The terminal voltage curve over this period is called reference discharge profile. By integrating the currents over this discharge period, the capacity of the battery ( $Q$ ) can be calculated. Fig. 3.7a shows the reference discharge profiles for battery B3 at different aging levels. The curves fade from black to red as the battery ages. Fig. 3.7b shows the capacity fade curve for this battery. It can be seen that the capacity gradually decreases over time.

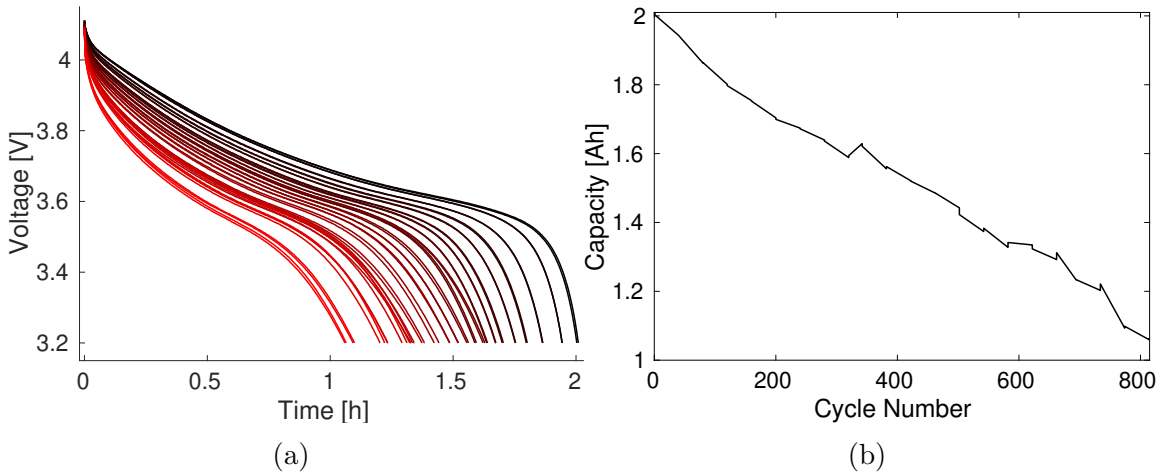


Figure 3.7: (a) Reference discharge profile for battery B3 (The curves fade from black to red as the battery ages. (b) Capacity fade curve for the battery B3.

### 3.5.2 Results and Discussion

#### SOH Estimation Results

By applying the proposed method to NASA degradation battery dataset for batteries B3, B13, B15, B16, B21, B22, and B23, the capacity  $Q$  of the batteries are estimated. SOH is estimated by normalizing estimated values of  $Q$  by  $Q_{rated}$  that is the capacity of a new unaged battery. The estimated degradation SOH curves over the batteries lifetimes are shown in Fig. 3.8. The red graphs are the estimated SOH curves based on the proposed method and the blue curves are SOH curves based on reference tests. In this figure, the  $x$  axis shows the discharge interval number.

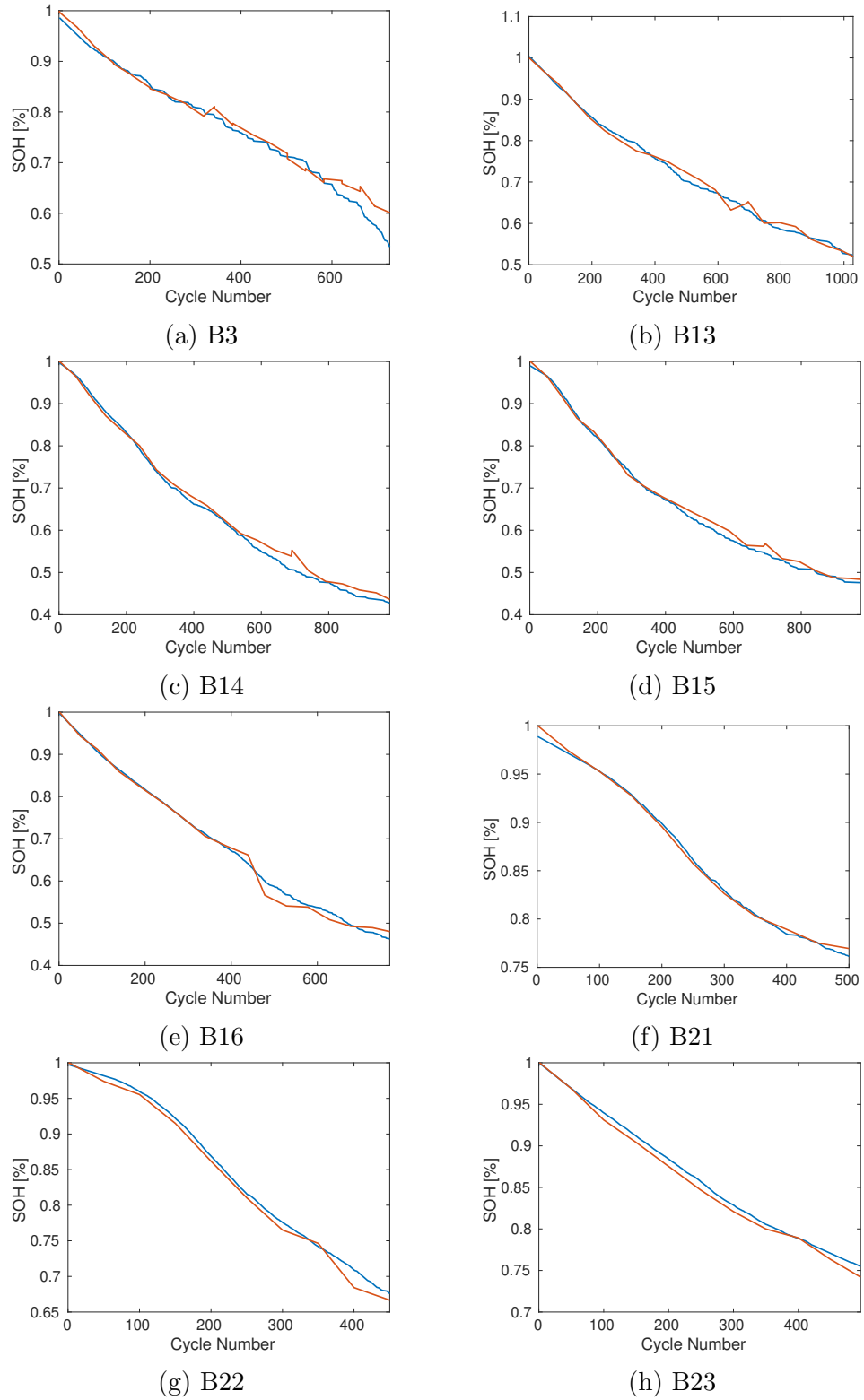
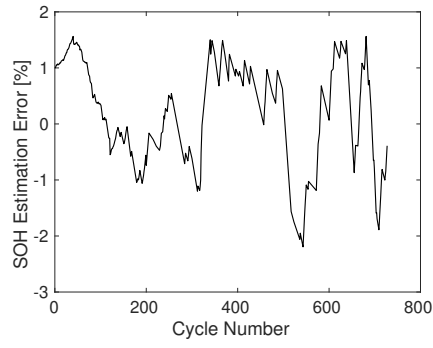
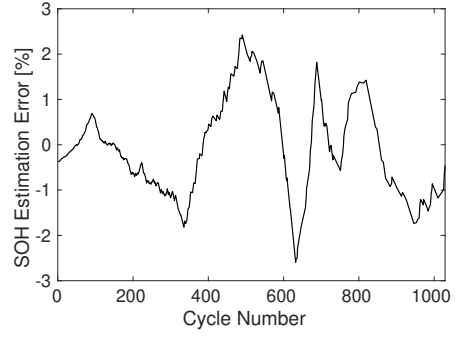


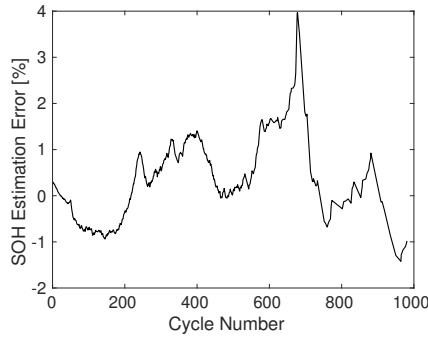
Figure 3.8: SOH estimation curves (blue plots) vs real SOH curves (orange plots).



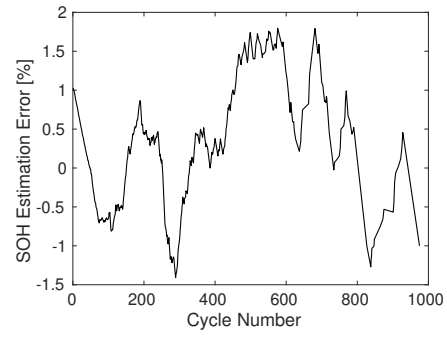
(a) B3



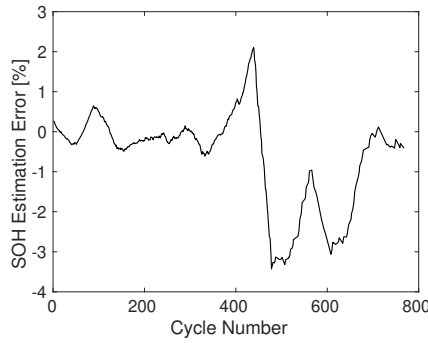
(b) B13



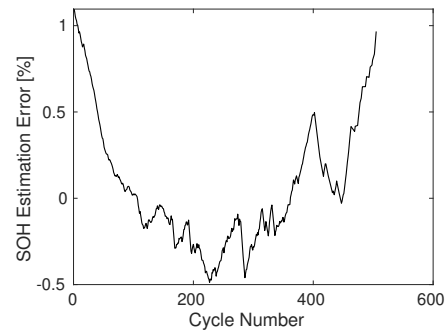
(c) B14



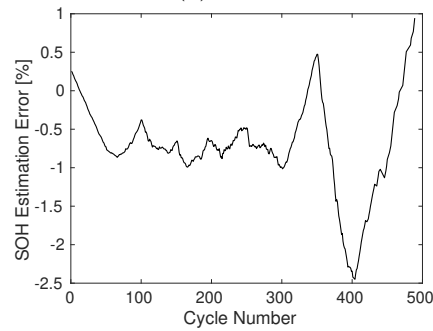
(d) B15



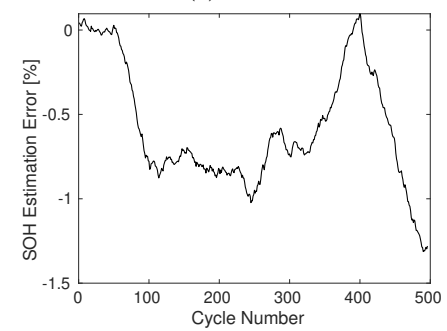
(e) B16



(f) B21



(g) B22



(h) B23

Figure 3.9: SOH estimation error curves.

The SOH estimation error curves are shown in Fig. 3.9. For batteries B3 and B15 the maximum error is 2% , for the batteries B13, B14, B16, and B22 the maximum error is 3%, and for the batteries B21 and B23 the maximum error is 1%, for 98.3% of intervals. In this work, root mean square error (RMSE) is used to evaluate the SOH estimations, which is defined as:

$$\text{RMSE} = \sqrt{\frac{1}{N} \sum_{i=1}^N (\text{SOH}_i - \hat{\text{SOH}}_i)^2}, \quad (3.8)$$

where  $N$  is the number of partial discharge intervals,  $\text{SOH}_i$  is the reference SOH value at interval  $i$ , and  $\hat{\text{SOH}}_i$  is the estimated SOH value at interval  $i$ . For all batteries, the root mean square error (RMSE) of the estimation is calculated and reported in Table 3.1. RMSE value for the majority of batteries, B3, B13, B14, B15, B21, B22, and B23 is less than 1% and for only one battery, B16 slightly higher than 1%, demonstrating the accuracy and robustness of the assumptions as well as the proposed method. Also, it should be mentioned that the estimated curves have been smoothed using Savitzky-Golay filter [53] that is a filter used for smoothing digital data.

Table 3.1: RMSE of the proposed method estimations

B#	B3	B13	B14	B15	B16	B21	B22	B23
RMSE	0.96%	0.88%	0.89%	0.8%	1.07%	0.37%	0.92%	0.67%

Table 3.3 compares the proposed method with other existing methods in literature. Generally, the methods that use offline training provide accurate results, and methods that do not use offline training have less accuracy and it is worth noting that although the proposed method does not use offline training, its results are comparable to the ones with offline training. The state of the art SOH estimation algorithms with offline training that have been studied in [17] including hybrid ensemble learning (HEL), extreme learning machine (ELM), random vector functional link (RVFL), support vector machine (SVM), echo state network (ESN), random forest (RF), and stacked denoising autoencoders (SDA) are also compared and listed in Table 3.3.

Table 3.2: Information regarding the dataset of the methods in literature [45]

Algorithm	No Offline Training	Dataset
Proposed method	YES	NASA RW
Proposed method	YES	NASA RW
Proposed method	YES	NASA RW
RLS-AHIF [45]	YES	Experimental DST
DEKF [54]	YES	Experimental DST
Multiscale DEKF [54]	YES	Experimental DST
Multiscale DEKF [55]	YES	Experimental DST
Multiscale DEKF [56]	YES	Experimental DST
FOC [48]	YES	Experimental HP
HEL, ELM, RVFL, SVM, ESN, RF, SDA [17]	NO	NASA RW

Table 3.3: Comparison between our proposed method and other methods in literature in terms of estimation RMSE, convergence time and initial capacity error(if applicable) for different types of datasets [45]

Algorithm	$Q$ Initial Error	Convergence Time	RMSE
Proposed method	10%	<10 sec	<1%
Proposed method	20%	<10 sec	<2%
Proposed method	30%	<10 sec	<5%
RLS-AHIF [45]	24%	<2 min	<6.5%
DEKF [54]	33%	<100 min	<3.2%
Multiscale DEKF [54]	33%	<100 min	<1.5%
Multiscale DEKF [55]	20%	<30 min	<7%
Multiscale DEKF [56]	37%	<10 min	<5%
FOC [48]	10%	<100 min	<1%
HEL, ELM, RVFL, SVM, ESN, RF, SDA [17]	-	-	<1%

On the other hand, some methods are completely online and are performed without any offline training. For example, fractional order calculus (FOC) [48] and multi-

timescale estimator (MTSE) [55] have achieved accurate estimations of SOH (within 1%). Compare to these algorithms, the proposed method in this thesis has the advantage of lacking the dependency to initial estimation errors based on the sensitivity analysis that will be explained in Section 3.5.4. For instance, in [48] if starting with large initial error, the capacity approaches the reference value within 6000 seconds. Also, [55] needs at least 1 hour for the capacity to approach the reference value. Another online method that has been introduced recently is based on RLS and adaptive HIF (RLS-HIF) joint estimation filters [45]. The SOH estimation dependency of different online methods on the initial capacity error has also been compared in Table 3.3. As can be seen in the table, there is a trade-off between the initial capacity error and the convergence time and the estimation error. The higher the initial capacity error, the more convergence time and the larger estimation error would be. RLS-AHIF was able to reach a short enough convergence time, but with 24% error in the initial capacity, the estimation error becomes 6.5% within 2 minutes. In addition to RLS-HIF algorithm, the estimation results for other algorithms such as dual extended Kalman filter (DEKF) and multi-scale DEKF are reported in Table 3.3. By three different initial values and different tuning of the parameters, three results for multi-scale DEKF are reported, indicating at least 10 minutes to converge. This means that if the circuit is disconnected or if due to some fault or overcurrent, the capacity changes, the re-estimation of the parameters needs another 10 minutes to converge, which might not be ideal.

### **SOC Estimation Results**

Based on the reference SOC-OCV curve and the estimated OCV, SOC can be estimated. Fig. 3.10 shows the estimated and reference SOC curves for a discharge interval in NASA dataset and its corresponding error curve. Also, RMSE of SOC estimations for all 8 batteries are reported in Table 3.4. The average SOC estimation error for all 8 batteries is 1.07%, which is acceptable for SOC estimation.

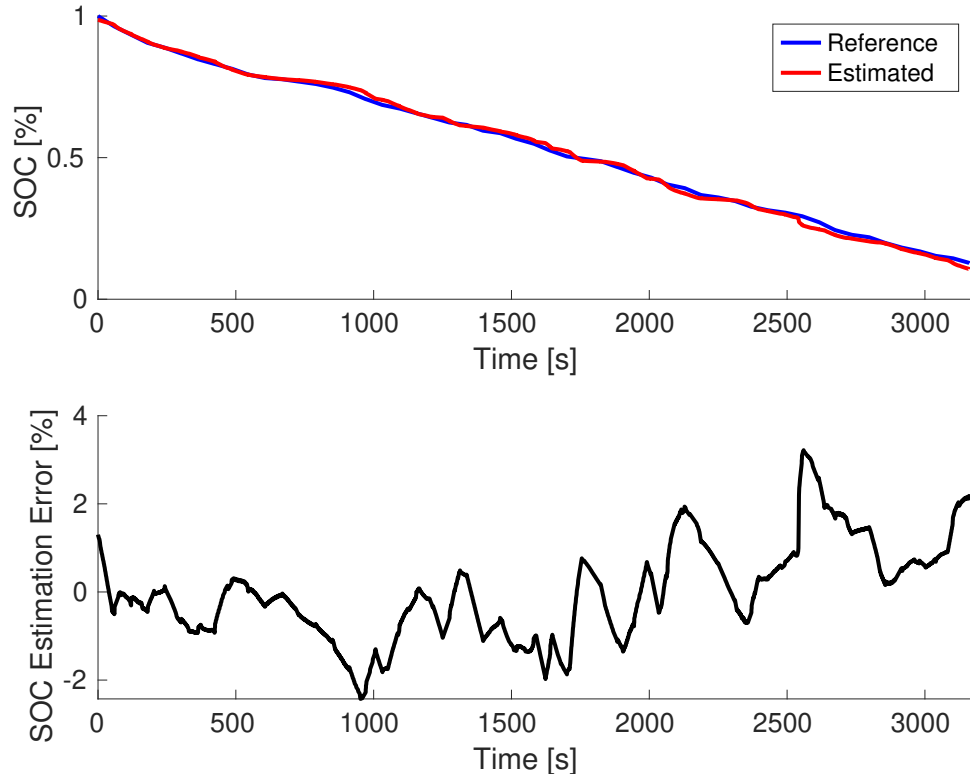


Figure 3.10: SOC estimation curve for a sample discharge interval in NASA data.

Table 3.4: RMSE of SOC estimations

B#	B3	B13	B14	B15	B16	B21	B22	B23
RMSE	1.46%	0.99%	1.24%	1%	1.3%	0.64%	1.1%	0.9%

### 3.5.3 Estimation Error Evaluation for Partial Discharge Intervals

As mentioned earlier in Section 3.4.1, the discharge intervals in NASA dataset are a combination of fully discharged and partially discharged intervals with partial intervals being the majority of them. In this section, the relationship between capacity estimation accuracy and the length of partial discharge intervals is evaluated. For each battery, the graph of SOH estimation errors with respect to the length of their respective partial discharge intervals is shown in Fig. 3.11.

As can be seen in Fig. 3.11, when the length of partial discharge intervals decreases, the accuracy of estimations decreases as well. Except for batteries B15, B16, the

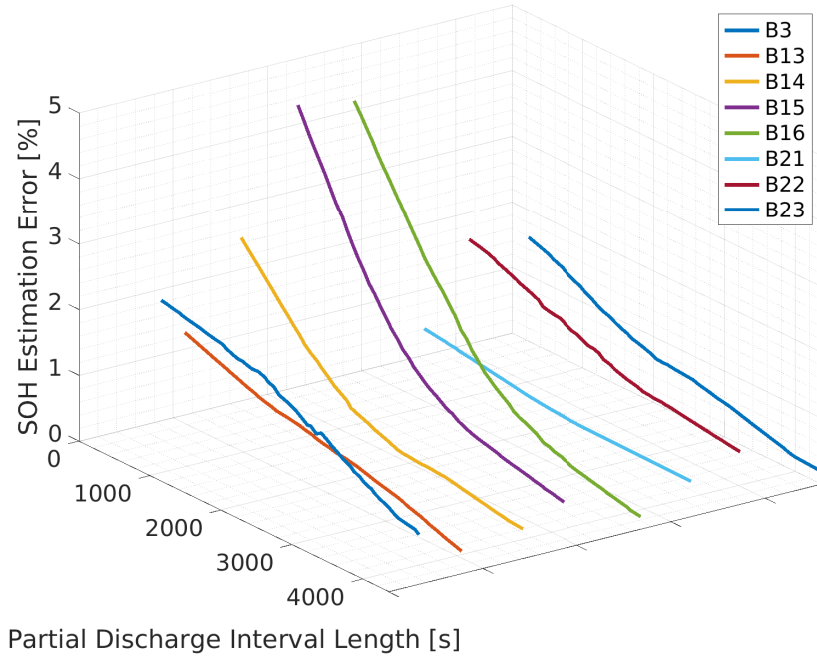


Figure 3.11: SOH estimation error curves based on the length of the partial discharge intervals.

maximum estimation error for other batteries is always below 2.5%, even for the lowest length intervals, which is an indication of the capability of the proposed method in online SOH estimation using partial discharge intervals.

### 3.5.4 Sensitivity Analysis

As mentioned in Section 3.2, the reference SOC-OCV curve used in this study is the estimated ISUM-OCV curve from the first two discharge cycles, normalized by a new battery rated capacity,  $Q_{rated}$ . If the data for the first two discharge cycles of the brand new battery is not available, then this reference curve cannot be obtained. In that case, the reference curve has to be estimated from the battery datasheet. Since batteries have manufacturing mismatches, the SOC-OCV curve from the datasheet will not be very accurate for all batteries. Therefore, the sensitivity of the SOH estimation results to the reference SOC-OCV curve need to be assessed.

An incorrect SOC-OCV curve is equivalent to a correct ISUM-OCV curve with an

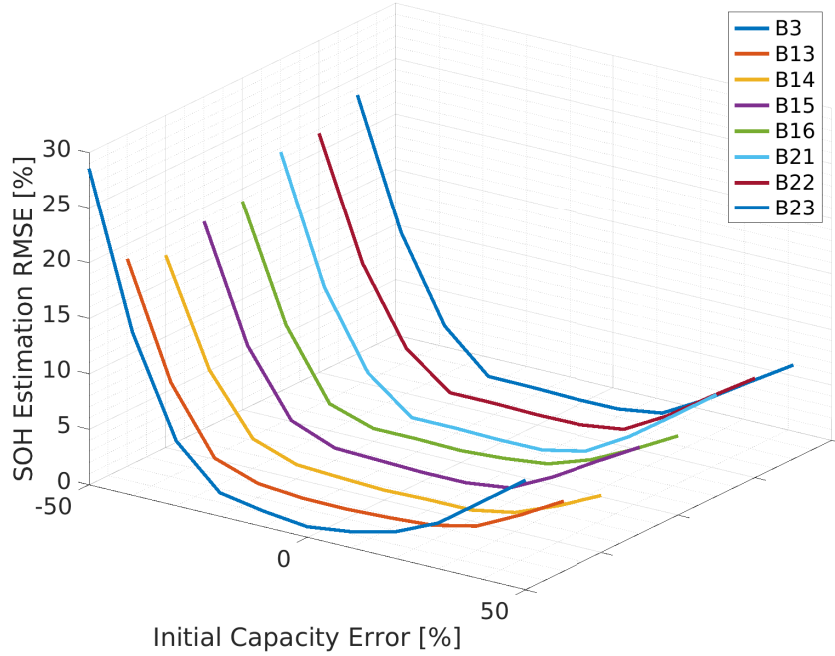


Figure 3.12: Sensitivity of SOH estimations to initial capacity ( $Q_{rated}$ ) error.

incorrect  $Q_{rated}$ , as SOC-OCV curve is in fact ISUM-OCV curve normalized by  $Q_{rated}$ . Therefore, for simplicity, instead of evaluating the sensitivity of SOH estimation to the reference SOC-OCV curve, its sensitivity to  $Q_{rated}$  will be evaluated. Fig. 3.12 shows the sensitivity of SOH estimation curves to  $Q_{rated}$  for all batteries. As can be seen, even  $\pm 10\%$  error in  $Q_{rated}$  still results in good estimations, mostly below 1%. For larger errors in initial capacity, such as  $\pm 20\%$  and  $\pm 30\%$ , the SOH estimation errors are below 2% and 5% respectively. These results are also represented in Table 3.3. Note that the SOH estimation errors for initial capacity errors until  $\pm 50\%$  are plotted in Fig. 3.12, showing the robustness of the proposed algorithm to the initial capacity error.

### 3.6 Conclusion

In this chapter, a new method for online estimation of Li Ion battery capacity, SOC, and SOH using partial discharge dataset was proposed. The parameters of battery

electrical circuit model (ECM) are estimated using two consecutive partial discharge intervals. NASA data sets are used to validate the proposed method. It is shown that the estimation error is around 1% based on 500 second partial discharge data. The parameter search was done by applying Adam optimization algorithm using Tensorflow package in Python. For each interval, the search was done within 10 seconds. Compared to other methods, the proposed online method exhibits faster convergence, much less sensitivity to initial capacity errors and high accuracy for partial discharge without offline trainings.

# Chapter 4

## Battery Status Estimation Considering Temperature

### 4.1 Introduction

The SOC-OCV relationship for a battery varies with temperature change. In Chapter 3, the SOC-OCV relationship for each battery was extracted based on the first two discharge cycles of that battery. Since the ambient temperature of each battery in NASA dataset was forced to be in a limited range at all cycles, therefore, SOC-OCV curve at all cycles is approximately the same for the same battery. As a result, the final reported SOH estimations based on the extracted reference SOC-OCV curve from the first two discharge cycles had relatively small errors. In reality, the first two discharge cycles of the batteries might not be available or accurate and that means the provided SOC-OCV curve from the datasheet needs to be used as reference. For such cases, since the operating temperature for the batteries in datasheet is 25 degrees, the provided curve needs to be adjusted for different temperatures.

In this chapter, we propose a method that improves the SOH estimations by considering the effect of temperature on SOC-OCV curves. In this method, first the reference curve at 25°C is extracted from the datasheet. Afterwards, a neural network is trained to estimate battery internal resistance based on temperature, SOC, and SOH. Finally, based on the estimated internal resistance from the trained neural network, SOC-OCV curve from the datasheet is modified for different temperatures

and new estimations of SOH based on these modified curves will be obtained. Note that if the reference SOC-OCV curves at temperatures other than 25°C were available in the datasheet, the neural network’s training would be unnecessary and one could use the provided reference curves at different temperatures for estimating SOH and skip this chapter.

The rest of this chapter is organized as follows. Section 4.2 explains how temperature can affect SOH. In Section 4.3, the proposed method will be explained. Section 4.4 provides the estimation results and Finally, Section 4.5 concludes this chapter.

## 4.2 Temperature Effect on Battery Parameters Estimation

Based on [57], SOC-OCV curves are different at various temperatures. As explained in the previous chapter, the capacity  $Q$  is estimated based on a reference SOC-OCV curve. Therefore, if the battery’s operating temperature is not close to the temperature in which the reference SOC-OCV curve was obtained, the estimated  $Q$  and therefore SOH would be erroneous. In Chapter 3, the reference SOC-OCV curve for each battery was obtained from the first two discharge cycles of that battery. Since the operating temperature for each battery in NASA dataset was held close to a constant temperature, therefore, the SOC-OCV curves for all of the discharge intervals of the same battery are approximately the same. Thus, there are little errors in the estimations based on the reference SOC-OCV curve, extracted from the first two cycles.

In practice, the data of the first two discharge cycles of the battery might not be available or the temperature of the first two cycle may change or it might not be desired to rely all the calculations based on two cycles measurements which may have noise or errors.

In such cases, one needs to use the reference curve from the battery datasheet. Since the reference SOC-OCV curve in the datasheet is obtained at 25°C, the SOH

estimations based on this curve are expected to be inaccurate, specially for those intervals that their temperature has larger distance from 25°C. Fig. 4.1 shows the estimated SOH curves for the batteries in NASA dataset, based on the datasheet’s reference SOC-OCV curve at 25°C. Also, Fig. 4.2 shows the error curves for these estimations and also the average temperature for each cycle is depicted as well. As can be seen, the results for battery B3 are not reported. The reason is that in NASA dataset, the temperature measurements for battery B3 were incorrect and therefore, battery B3 will not be used in this chapter.

In Fig. 4.2, the red horizontal lines in the temperature plots indicate 25°C. The farther the temperature from this line, the more error in SOH estimations is expected, as the reference SOC-OCV curve is obtained at 25°C. As can be seen in Fig. 4.1, 4.2, the SOH estimations for batteries B13, B14, B15, and B16 are rather good. This is because the operating temperature for all these batteries is around 25°C, which is the same temperature as the reference SOC-OCV curve. However, the results are still not as good as the results of the previous chapter, as those results used specific SOC-OCV curves for each battery, extracted from their own discharge intervals, based on their first two cycles. Based on Fig. 4.2, as expected, the SOH estimation for batteries B21, B22, and B23 are highly inaccurate, considering the operating temperatures of these batteries have a large distance from 25°C. The numerical SOH estimation results based on the datasheet’s reference curve at 25°C, are reported in Table 4.1.

Table 4.1: RMSE of SOH estimations using reference SOC-OCV curve from the datasheet

B#	B13	B14	B15	B16	B21	B22	B23
RMSE without temperature	4.33%	2.61%	2.01%	3.73%	7.94%	5.33%	6.73%

Based on the above results, the SOC-OCV curves need to be adjusted for different temperatures, so that the SOH can be estimated accurately. Since the SOC-OCV curve is not available at all temperatures, a method is required to produce SOC-OCV

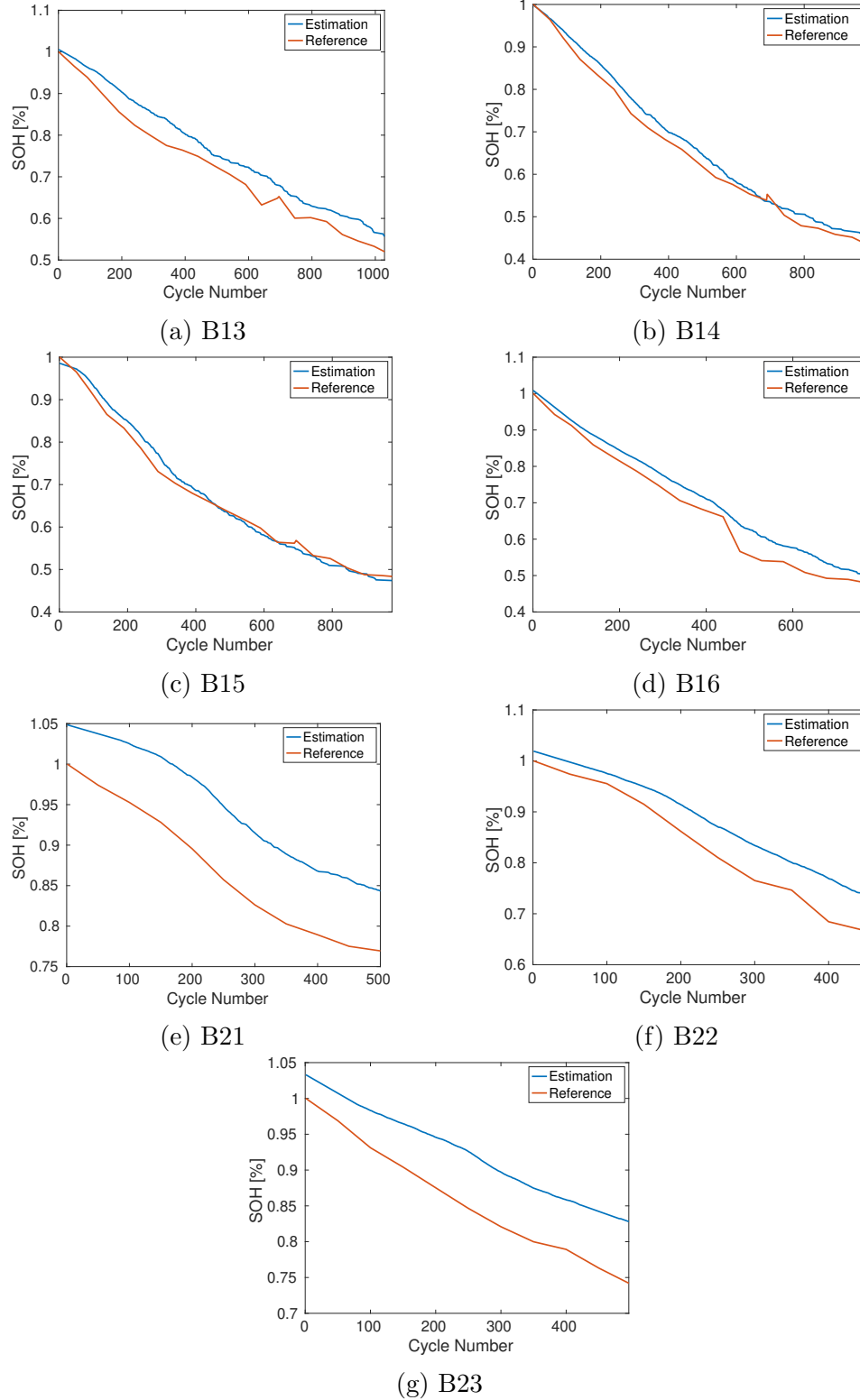
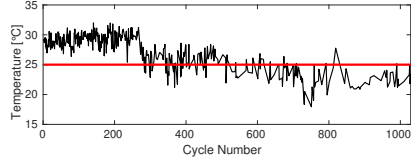
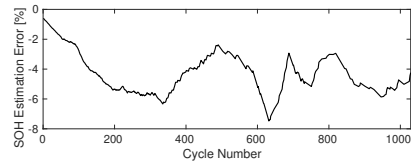
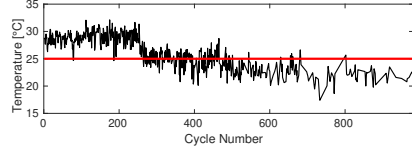
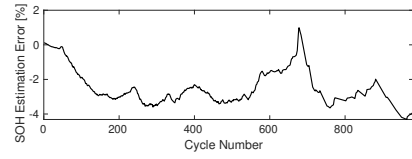


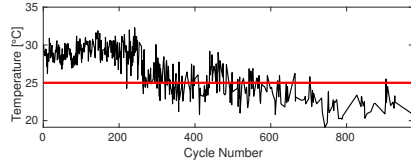
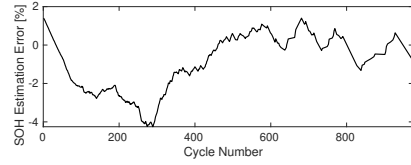
Figure 4.1: SOH estimation curves (blue plots) using datasheet's data at 25°C as the reference SOC-OCV curve vs reference SOH curves (orange plots).



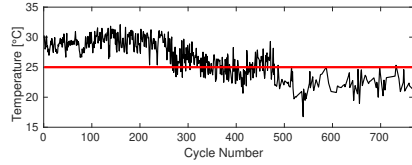
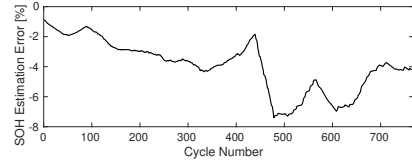
(a) B13



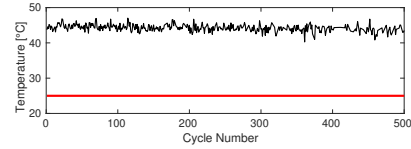
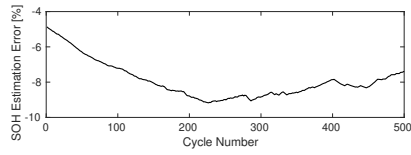
(b) B14



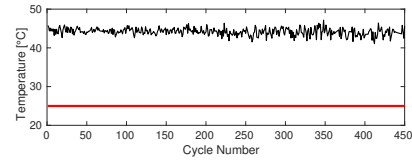
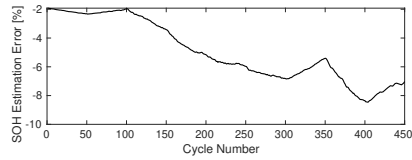
(c) B15



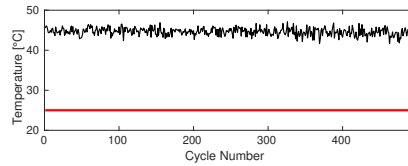
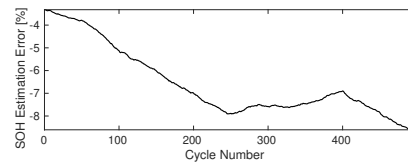
(d) B16



(e) B21



(f) B22



(g) B23

Figure 4.2: SOH estimation error curves and temperatures using datasheet's data at 25°C as the reference SOC-OCV curve.

curve for every temperature. In the next section, a proposed method will be provided to achieve this goal.

## 4.3 The Proposed Method

As explained in Section 4.2, ignoring the effect of temperature in SOH estimation will lead to inaccurate results. Therefore, in this section, a method will be proposed to estimate SOH by considering the ambient temperature effect. First, an overview of the proposed method will be provided and afterwards, the proposed method will be explained in details.

### 4.3.1 Problem Definition

The main goal is to identify the reference SOC-OCV curves at all temperatures based on the information in the battery datasheet. Fig. 4.3, 4.4 depict all the discharge profiles provided in the Li-ion battery datasheet [25]. Since these discharge profiles show the battery terminal voltage  $V_T$  and not OCV, the effect of other parameters should be removed from the terminal voltage to extract OCV. The overview of the proposed method for estimating SOC-OCV curve based on the discharge profiles in the datasheet is as follows:

(i) Estimating battery steady state internal resistance at the nominal temperature of 25°C: based on the datasheet provided curves as shown in Fig. 4.3. The steady state internal resistance  $R_0$  is the summation of the internal resistance and the polarization resistance:  $R_0 = R_s + R_p$ .

(ii) Estimating SOC-OCV curve at the nominal temperature of 25°C: by removing the effect of the steady state internal resistance from the discharge profiles provided in Fig. 4.3.

(iii) Deriving a model to estimate battery steady state internal resistance as a function of temperature

(iv) Estimating SOC-OCV curves for extreme temperatures: by removing the effect of the steady state internal resistance from the discharge profiles in Fig. 4.4.

(v) Incremental modeling of SOC-OCV curves for any temperature between extreme temperatures of  $55^{\circ}\text{C}$  and  $-20^{\circ}\text{C}$ .

These steps will be further explained in details in the next section.

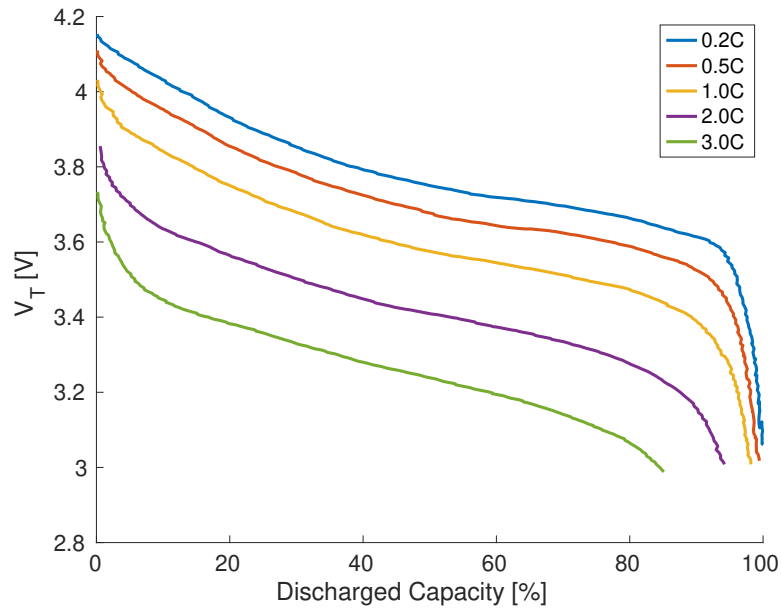


Figure 4.3: Datasheet discharge curves with different discharge currents at  $25^{\circ}\text{C}$ .

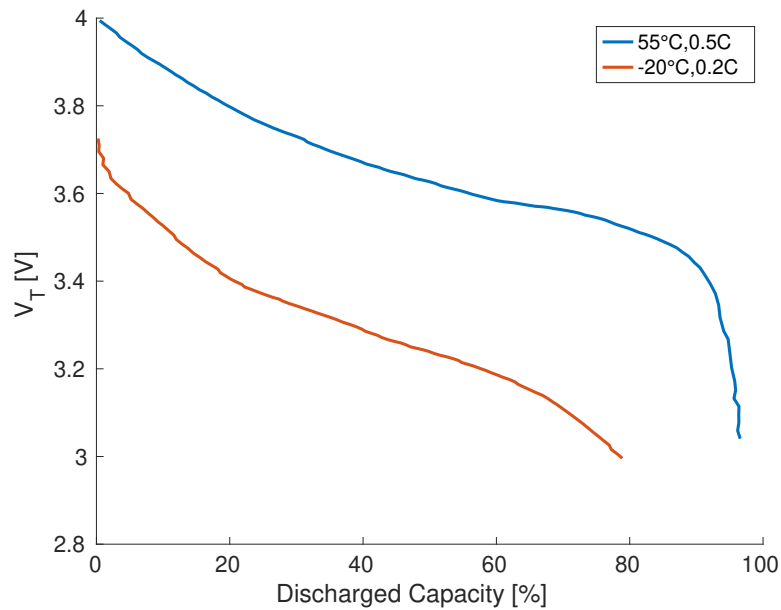


Figure 4.4: Datasheet discharge curves at different temperatures.

### 4.3.2 Details of the Proposed Method

#### (i) Estimating Battery steady state internal resistance at the nominal temperature of 25°C

Fig. 4.3 shows the provided curves at 25°C from the 18650 Li-ion battery datasheet [25]. It shows the terminal voltage of the battery when discharging with 5 different currents, where  $C$  is the standard discharge current in the datasheet, which is 0.52A. The charging temperature is 25°C. Based on (2.13), the terminal voltage consists of three separate additive components, OCV,  $-R_s I_L$ , and  $V_p$ . According to 2.14,  $V_p$  is equal to  $-R_p I_L$  at steady state. Therefore, at steady state, the terminal voltage is:

$$V_T = V_{oc} - R_s I_L - R_p I_L = V_{oc} - R_0 I_L, \quad (4.1)$$

where  $R_0$  is the summation of the battery internal resistance  $R_s$  and the polarization resistance  $R_p$ , and is called the "steady state internal resistance" in this thesis.

Based on (4.1), at a constant temperature, the difference between any two terminal voltage curves in Fig. 4.3 is equal to  $R_0 \Delta I_L$ , where  $\Delta I_L$  is the difference between the discharge currents of those curves. Therefore, by subtracting any of those discharge profiles from each other and dividing the result by  $\Delta I_L$ ,  $R_0$  can be estimated. Eventually, by adding the estimated  $R_0 I_L$  to the discharge profiles, OCV curve will be estimated.

#### (ii) Estimating SOC-OCV curve at the nominal temperature of 25°C

There are 5 discharge curves in Fig. 4.3 and that will provide  $\binom{5}{2} = 10$  different estimations for OCV curve, which are depicted in Fig. 4.5. The more current flows through the battery, the higher its temperature will get. Therefore,  $R_s$  and  $R_p$ , which are both functions of temperature, will vary for different discharge currents. This fact explains why the estimated OCV curves in Fig. 4.5 are slightly different, while based on assumption 2 (Section 3.3.2) the OCV-SOC curves should be constant for the similar temperatures throughout the life time of a battery.

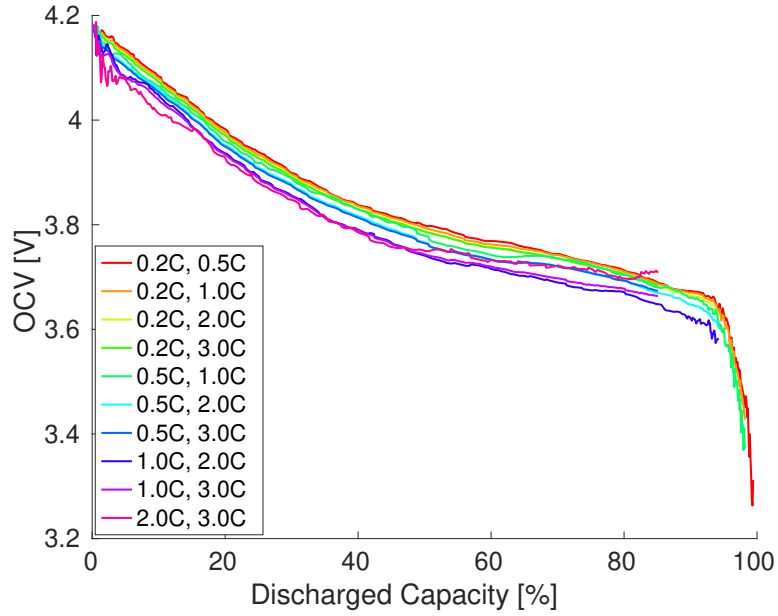


Figure 4.5: OCV curves estimations from the provided discharge curves in the datasheet as illustrated in Fig. 4.3.

The first SOC-OCV curve in Fig. 4.5 is used as the reference SOC-OCV curve at 25°C, because the discharge currents 0.2C, 0.5C are lower than other currents and have lower difference from each other, therefore the temperature does not increase as much and remains closest to 25°C.

### (iii) Deriving a model to estimate battery steady state internal resistance as a function of temperature

The provided datasheet discharge profiles at temperatures other than 25°C are illustrated in Fig. 4.4. As can be observed, there are only two discharge profiles, at temperatures 55°C and -20°C, with discharge currents 0.5C and 0.2C respectively. Since only one discharge curve is provided for each temperature, 55°C, -20°C,  $R_0$  cannot be estimated based on these curves and therefore SOC-OCV curves at temperatures other than 25°C cannot be directly extracted from the datasheet. If multiple discharge curves at these temperatures were provided in the datasheet, the steady state internal resistance could be estimated similar to the estimating at 25°C, as explained in part (ii). In that case, one can skip this part and directly jump to the next part.

In the case of 18650 Li-ion battery, as mentioned above, only one discharge curve is available in datasheet at 55°C and -20°C and therefore, the rest of this part should be followed.

For extracting OCV out of the terminal voltage of these discharge profiles, for various temperatures, the effect of  $R_0$  needs to be removed from the terminal voltage, according to (4.1). Since  $R_s$ ,  $R_p$  are variant with temperature,  $R_0$  value is unknown and needs to be estimated. In Part (i),  $R_0$  at 25°C was estimated. In this section, a model will be developed to estimate  $R_0$  at different temperatures based on its known value at an arbitrary temperature, which in this case is 25°C.

In order to find a model that relates the steady state internal resistance with the temperature, either a physical experiment or a large set of data is needed to train the model. In this thesis, the latter approach will be used. Since in Chapter 3, the steady state internal resistance  $R_0$  was estimated during the discharge intervals and the temperature was measured, these information can be used for training the model. Note that since the estimation of  $R_p$  and  $R_s$  in Chapter 3 were done based on two consecutive discharge cycles in which the temperature had little variations, they are reliable to be used here. The steady state internal resistance is also a function of SOC and SOH besides temperature:

$$R_0 = h(\text{SOC}, \text{SOH}, T). \quad (4.2)$$

Therefore, the model's inputs are the battery SOC, SOH, and temperature, and the model's output is its steady state internal resistance  $R_0$ . A neural network is trained to find the relationship between these inputs and the output. The discharge data of battery B14, B15 in NASA dataset are used to train a neural network for finding function  $h$  in (4.2). The details regarding the training of the neural network are provided in Appendix A.

After finding the function  $h$ , by setting the SOH=100%,  $R_0$  can be obtained as a function of temperature at any constant SOC. Fig. 4.6 shows the estimated steady

state internal resistance  $R_0$  graph with respect to the temperature at 5 different SOC's for battery B14, B15:

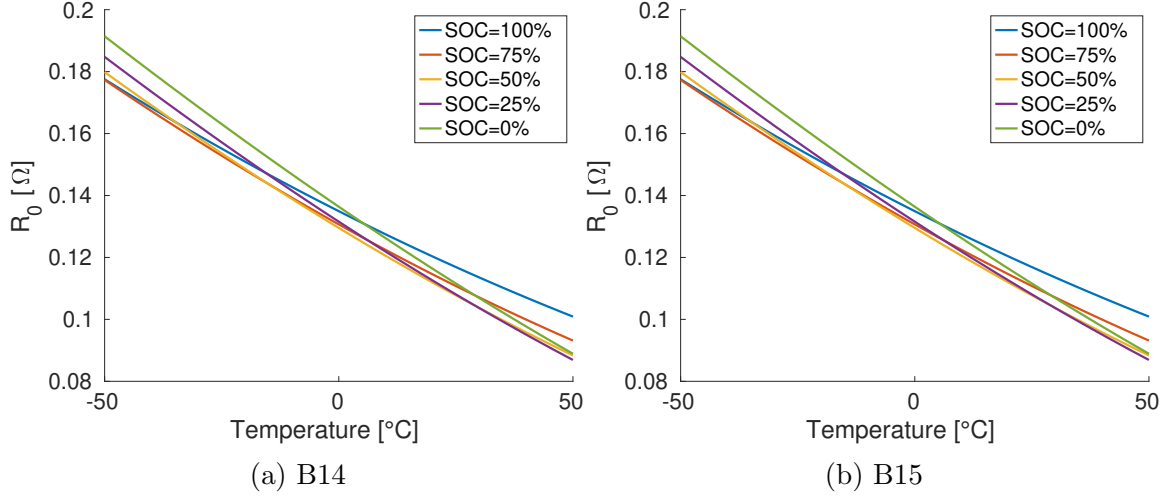


Figure 4.6: The steady state internal resistance variation with temperature at 5 different SOC's for battery (a) B14, (b) B15.

Based on Fig. 4.6, the relationship between  $R_0$  and temperature is linear at all SOC's. The average slope of battery B14 curves is  $-0.9\text{m}\Omega/^{\circ}\text{C}$  and the average slope of the curves of the battery B15 is  $-0.88\text{m}\Omega/^{\circ}\text{C}$ . Since the slope of the curves are approximately the same, it is safe to assume that the slope of  $R_0$  variation with respect to temperature for all Li-ion batteries is about the same as the respective slope for batteries B14, B15. Therefore, in this study,  $m = -0.9\text{m}\Omega/^{\circ}\text{C}$  will be used as the slope of the internal resistance variation with respect to the temperature.

#### (iv) Estimating SOC-OCV curves for extreme temperatures

Based on the slope  $m$ , by knowing the value of  $R_0$  at a given temperature  $T_0$ ,  $R_0$  can be estimated at any other temperature ( $T$ ) as:

$$R_0(T) = R_0(T_0) + m(T - T_0). \quad (4.3)$$

Therefore, using the estimated slope  $m = -0.9\text{m}\Omega/^{\circ}\text{C}$  and the estimated  $R_0$  at  $25^{\circ}\text{C}$  in Part (i), the internal resistance can be estimated for two extreme temperatures of  $55^{\circ}\text{C}$  and  $-20^{\circ}\text{C}$ . By removing the effect of  $R_0$  from the discharge profiles of Fig. 4.4,

SOC-OCV curve will be estimated at temperatures 55°C and -20°C. Fig. 4.7 shows these two curves.

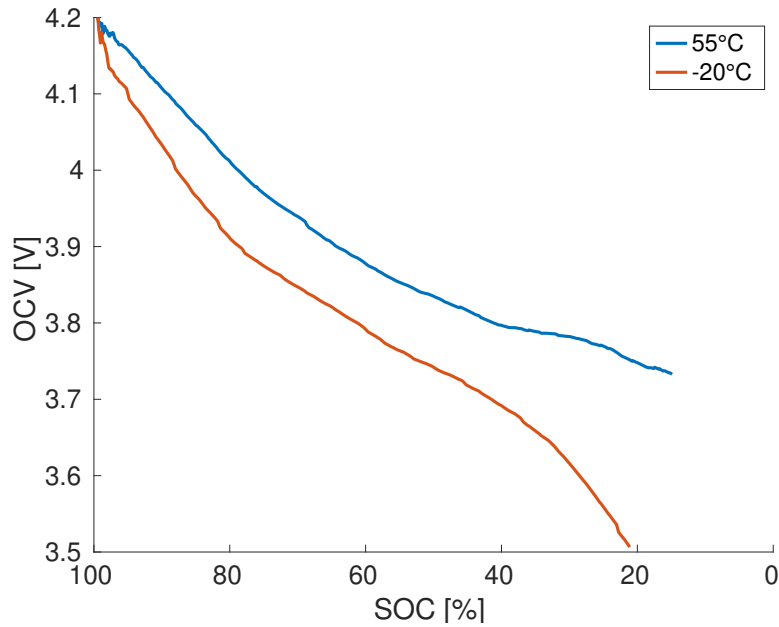


Figure 4.7: The estimated SOC-OCV curves at 55°C and -20°C

**(v) Incremental modeling of SOC-OCV curves for any temperature between extreme temperatures of 55°C and -20°C**

Based on the estimating SOC-OCV curves at 55°C and -20°C, shown in Fig. 4.7, it can be seen that the SOC-OCV curves at the higher temperatures lie above the curves at the lower temperatures. Therefore, it is predictable that using SOC-OCV curve at one temperature as a reference curve for all temperatures would lead to incorrect capacity  $Q$  and therefore SOH estimations, as it was seen in Section 4.2. Thus, the reference SOC-OCV curve should be adjusted for every temperature.

To improve the SOH estimation results, an approximate adjustment of the reference SOC-OCV for each temperature will suffice. Therefore, it is proposed to assume a linear relationship between OCV change at any given SOC with temperature. As a result, by calculating the difference between SOC-OCV curves at 55°C and -20°C, shown in Fig. 4.7, the OCV change with respect to temperature at all SOCs will be estimated. The resulting curve is depicted in Fig. 4.8.

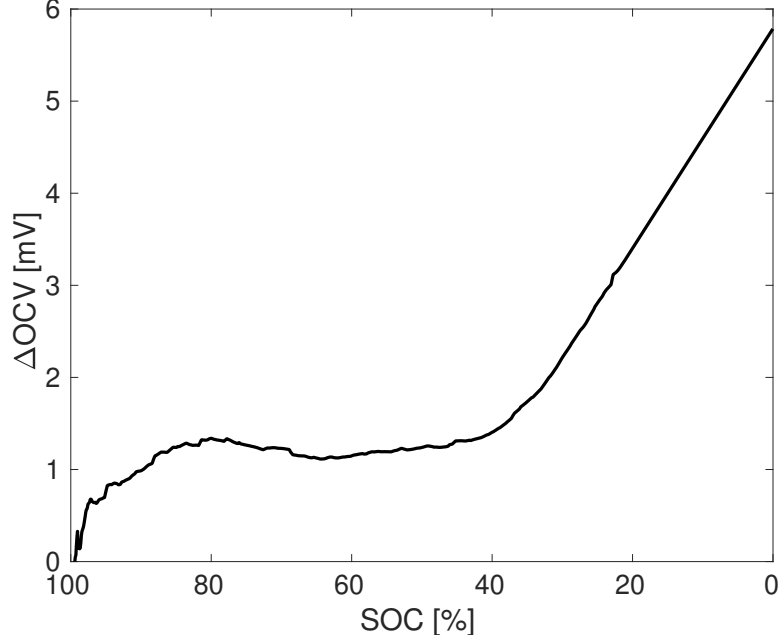


Figure 4.8: OCV variation for 1°C temperature increase

### 4.3.3 Summary of the Proposed Method

As explained in the previous section, the proposed method uses the battery datasheet to estimate SOC-OCV curve and the internal resistance of the battery at 25°C. Also, it trains a neural network to find the relationship between the battery internal resistance and temperature. Next, it uses the trained network to estimate its internal resistance at extreme temperatures of 55°C and -20°C. Using these estimations, the effect of internal resistance will then be removed from the battery terminal voltages at the extreme temperatures and therefore, SOC-OCV curves at these extreme temperatures will be estimated. By calculating the difference between SOC-OCV curves at the extreme temperature and dividing the result by the difference between extreme temperatures, OCV change as a function of SOC for 1°C temperature variation will be derived. Using the derived curve, SOC-OCV curve at any temperature can be estimated and the new SOH estimations can be done with the temperature-compensated SOC-OCV curves. The flowchart of the proposed algorithm is presented in Fig. 4.9.

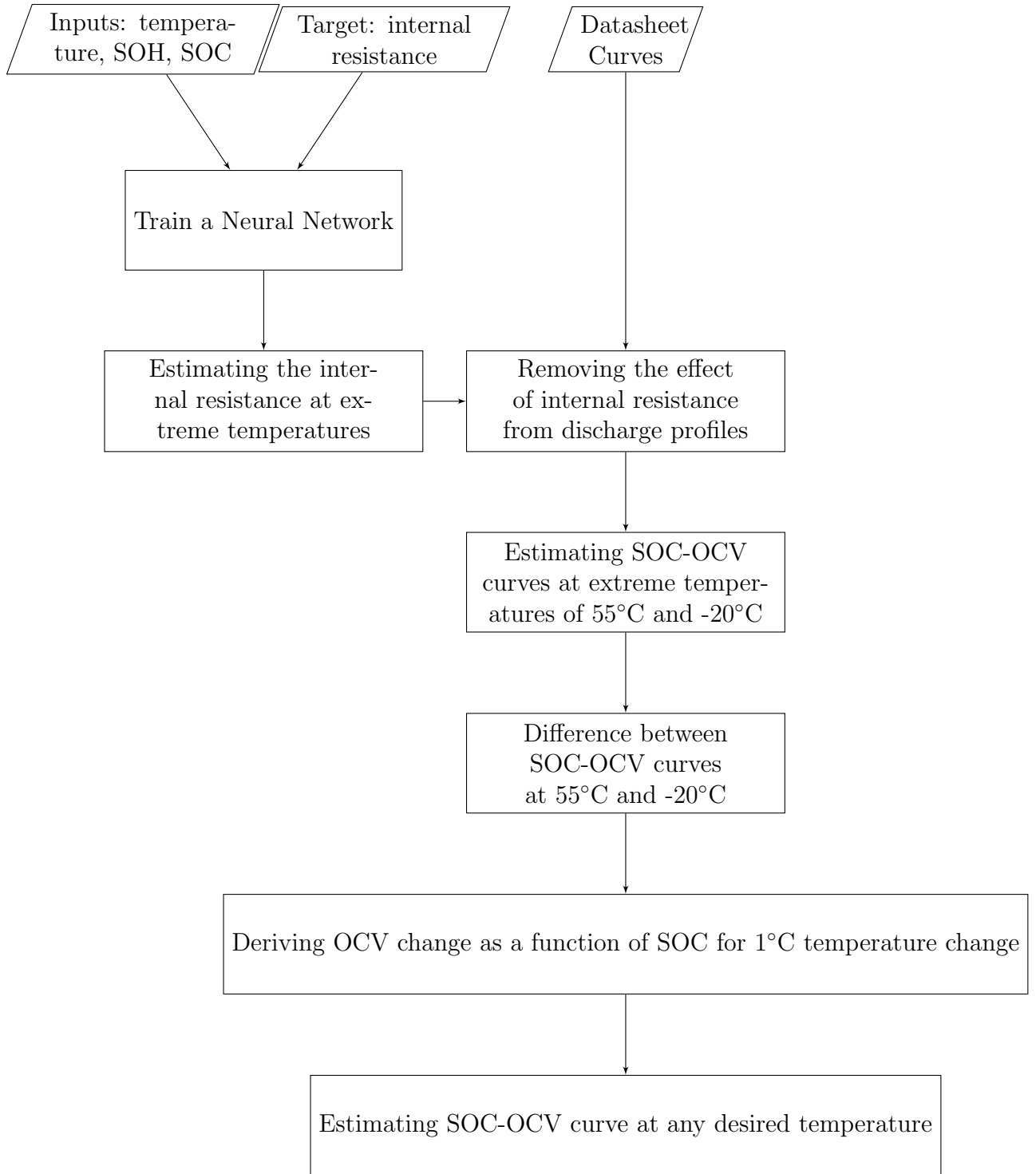


Figure 4.9: Flowchart of the proposed algorithm

## 4.4 Estimation Results

Using the estimated curve shown in Fig. 4.8 and adjusting the SOC-OCV curve for every temperature,  $Q$  and SOH can be estimated more accurately. Fig. 4.10 shows the SOH estimation results using the adjusted SOC-OCV curves for batteries B13, B14, B15, B16, B21, B22, and B23. The error curves are also depicted in Fig. 4.11. Based on these results, it is evident that the estimations have been improved significantly compared to the case when only one reference SOC-OCV curve was used for every temperature.

The numerical results are reported in Table 4.2. As can be seen, the SOH estimation RMSE has been improved by 2.55% on average. It can be seen that batteries B21, B22, and B23 have significant improvements in their estimations. This is because their ambient temperature were around 45°C and therefore, it is only reasonable that using a reference SOC-OCV curve obtained at 25°C would lead to large errors in the estimations.

## 4.5 Conclusion

In this chapter, a new method is proposed to adjust the reference SOC-OCV curve for any temperature to improve the battery SOH estimation in Chapter 3. The discharge profiles provided in Li-ion battery datasheet are used to find a reference SOC-OCV curve at 25°C. For estimating SOC-OCV curve at other temperatures, first, a neural network was trained to find the relationship between the battery internal resistance and the temperature, using NASA dataset. Then, the estimated internal resistances at different temperatures were used to predict SOC-OCV curves for any given temperatures out of the provided curves in datasheet. It was shown that even for NASA dataset with almost constant temperature, the adjusted SOC-OCV curves improved the SOH estimations by 2.55% on average. For harsher circumstances, the proposed method is expected to significantly improve the estimations.

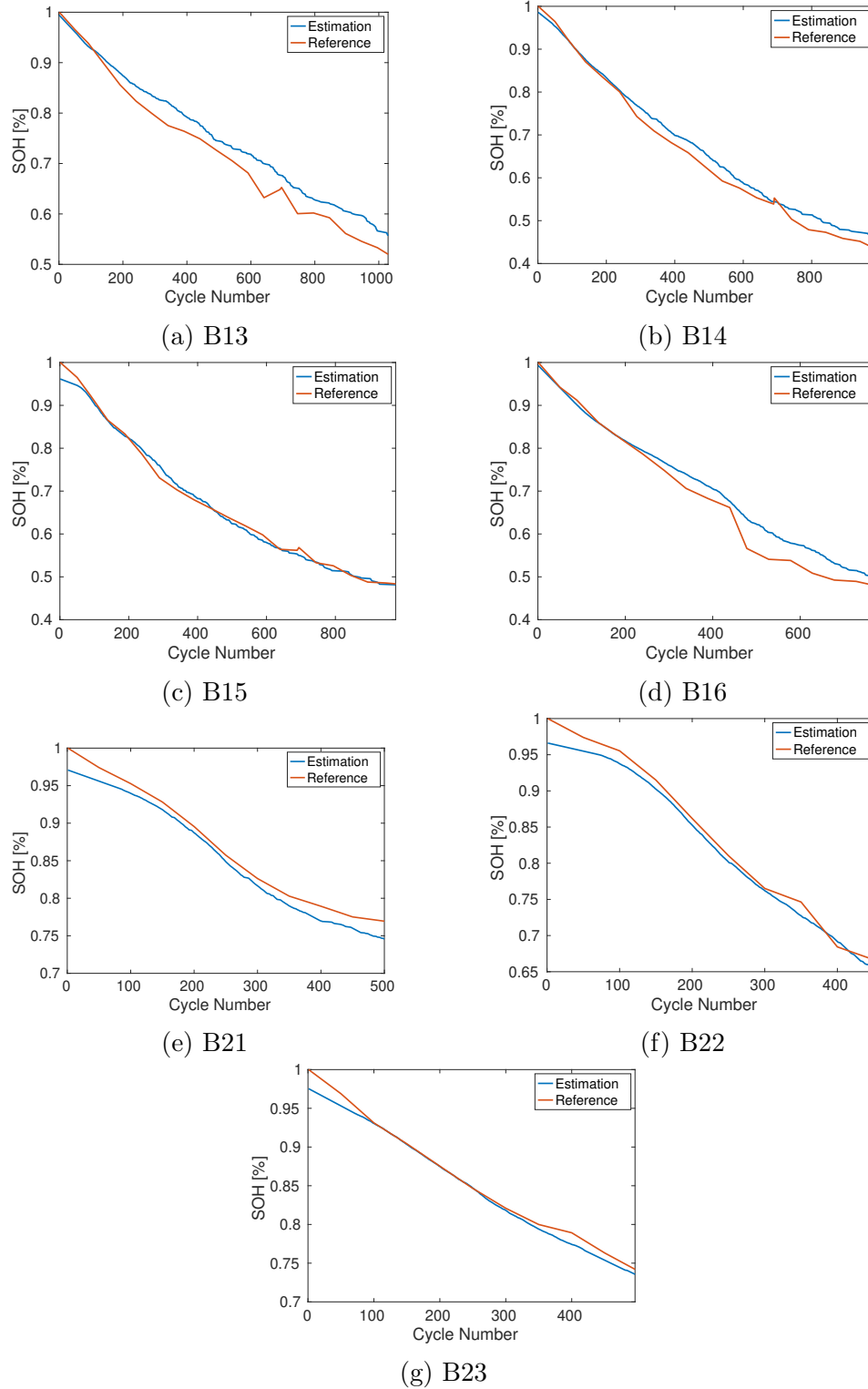
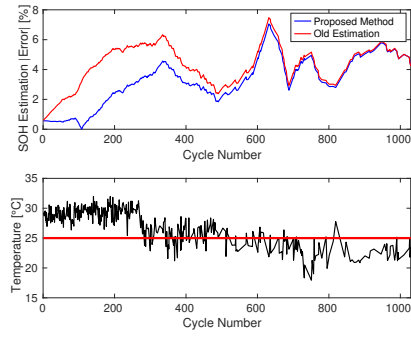
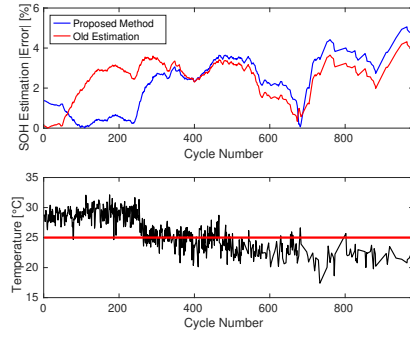


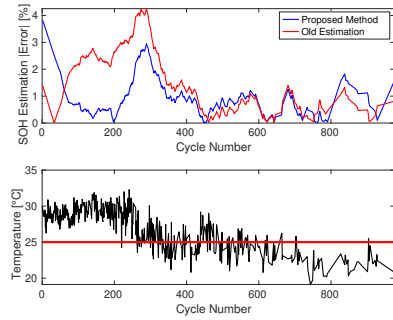
Figure 4.10: SOH estimation curves (blue plots) using temperature compensated SOC-OCV curves vs reference SOH curves (orange plots).



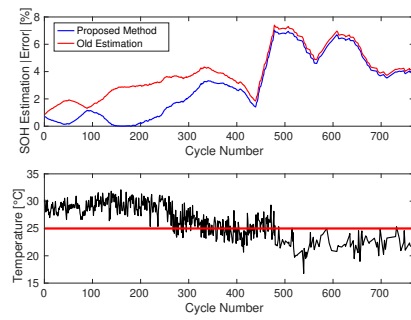
(a) B13



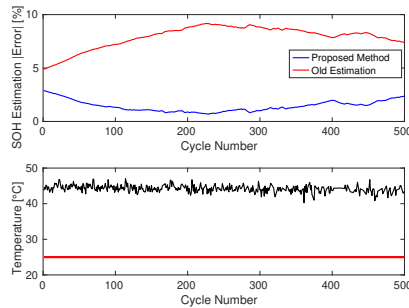
(b) B14



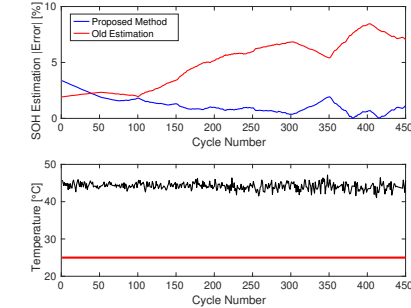
(c) B15



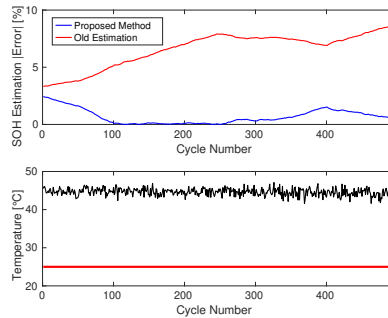
(d) B16



(e) B21



(f) B22



(g) B23

Figure 4.11: SOH estimation error curves and temperatures. Error curves for both cases are drawn: (i) using the temperature compensated SOC-OCV curves (blue plots), (ii) using only one SOC-OCV curve for all temperatures (red plots)

Table 4.2: RMSE of SOH estimations using reference SOC-OCV curve from the datasheet for two cases: (i) without considering the effect of the temperature, (ii) with considering the effect of the temperature. Also, the SOH estimation RMSE improvement is reported in the last row. The first and the second rows indicate the battery number and the RMSE of temperature difference with 25°C for each battery respectively

RMSE \ B#	B13	B14	B15	B16	B21	B22	B23
Temperature deviation from 25°C	3.55	3.2	3.4	3.49	19.24	19.16	16.64
SOH estimation without temperature compensation	4.33%	2.61%	2.01%	3.73%	7.94%	5.33%	6.73%
SOH estimation with temperature compensation	2.96%	2.24%	1.4%	2.94%	1.51%	1.44%	0.93%
SOH estimation improvement	1.37%	0.37%	0.61%	0.79%	6.43%	3.89%	5.8%

# Chapter 5

## Conclusions and Future Work

### 5.1 Summary of Works

In this work, Li-ion batteries were studied. The high price and growing demand of Li-ion batteries creates the necessity for battery management systems (BMS) to monitor batteries throughout their operation in order to prevent undesirable outcomes that might lead to significant financial damage.

The estimation of state of health (SOH) and state of charge (SOC) of batteries are two critical tasks of a BMS. The accurate estimations of SOH and SOC can ensure safe and stable operation of the battery and prevent the undesirable outcomes and therefore, prolong its lifetime. The main objective of this thesis was to efficiently and accurately estimate the SOH and SOC of the Li-ion battery, online and in various environmental conditions.

In Chapter 2, backgrounds regarding technical definitions of SOC and SOH of the batteries were explained. Also, equivalent circuit models (ECM) of Li-ion batteries were introduced and the first order ECM was selected to be the ECM using in this thesis. Adam optimization algorithm and neural networks were also introduced in Chapter 2 to be used later in Chapters 3, 4.

In Chapter 3, a new proposed method for online estimation of Li-ion battery SOC and SOH using partial discharge/charge data was introduced. In this method, Li-ion battery first order ECM is used to model the battery behaviour. The parameters of

ECM were estimated continuously, based on the data of the last two discharge/charge cycles of the battery, using Adam optimization algorithm. After estimating the parameters of ECM, SOH of the battery was estimated by comparing the estimated open circuit voltage (OCV) with the reference OCV curve, extracted either from the battery datasheet or the first two fully discharged cycles of the battery. SOC was also estimated based on the estimated OCV. NASA degradation dataset was used to validate the proposed method. The average SOH and SOC estimations RMSE on the batteries in NASA dataset for the proposed method were 0.82% and 1.07% respectively. The minimum required length for partial discharge intervals was considered 500 seconds and all the estimations have been done in less than 10 seconds for each interval.

In Chapter 4, the effect of temperature on the accuracy of SOH estimation was evaluated. In that chapter, instead of using the reference SOC-OCV curve extracted from the first two discharge cycles of each battery, the information was extracted from the battery datasheet. The reason behind this was to generalize the method for the cases when the data of the first two cycles of the battery are not available or contain noises. Also, since the operating temperature of each battery in NASA dataset was almost remained constant, the temperature of the first two discharge cycles of each battery are similar to their other cycles. Therefore, the effect of temperature variation on the estimations could not be shown properly with the extracted reference curves from the first two discharge cycles of each battery. Since the reference SOC-OCV curve in the datasheet was derived at 25°C, the estimation results for higher and lower temperatures than 25°C had errors. By training a neural network, a model for the internal resistance variation with respect to the temperature was derived for Li-ion batteries. That model was used to extract the SOC-OCV for different temperatures from the battery datasheet. With those new reference curves at various temperatures, new estimations for NASA dataset SOH were obtained and the estimation error was improved from 4.67% to 1.92%.

## 5.2 Future Work

In this thesis, the SOH and SOC of Li-ion batteries were estimated online using partial discharge and charge data and at various temperatures. NASA dataset was used to find a model that relates the battery internal resistance with the temperature. Since the batteries in NASA dataset have a limited range of operating temperature, the extracted models from this dataset might not be completely accurate. A possible future work is to perform comprehensive experiments at a wide range of operating temperatures and to find a more accurate “temperature-internal resistance” model and therefore, improve the SOH estimation results achieved in Chapter 4.

Another possible future work is using metaheuristic methods such as genetic algorithm [58], differential evolution [59], particle swarm optimization [60], ant colony optimization [61], simulated annealing [62], etc. instead of Adam optimization algorithm in Chapter 3 for estimating the parameters of the battery ECM. The advantage of using these metaheuristic methods is that the number of parameters in the optimization process can be increased and therefore, the accuracy of estimations may also increase.

Furthermore, using more than two consecutive discharge cycles for estimating the parameters of ECM certainly increases the accuracy of estimations. Using more than two cycles would minimize the effect of noises on the estimation and leads to more reliable results. However, this approach requires more data, which might not be ideal.

Another possible future work is estimating other performance indicators of the battery such as state of energy [63], state of power [64], state of function [65], etc. using the proposed method in this thesis. Using the estimated SOH and SOC of our proposed method for balancing the load distribution on multi-cell batteries is another potential future work. Cell balancing is of extreme importance in energy storage systems, as it enables the battery packs to exploit their maximum capacity and also prevents the capacity degradation, which prolongs the lifetime of the batteries [66],

[67].

# Bibliography

- [1] Y. Liang, C.-Z. Zhao, H. Yuan, Y. Chen, W. Zhang, J.-Q. Huang, D. Yu, Y. Liu, M.-M. Titirici, Y.-L. Chueh, *et al.*, “A review of rechargeable batteries for portable electronic devices,” *InfoMat*, vol. 1, no. 1, pp. 6–32, 2019.
- [2] G. Pistoia, *Lithium-ion batteries: advances and applications*. Newnes, 2013.
- [3] J. Speirs, M. Contestabile, Y. Houari, and R. Gross, “The future of lithium availability for electric vehicle batteries,” *Renewable and Sustainable Energy Reviews*, vol. 35, pp. 183–193, 2014.
- [4] C. Curry, “Lithium-ion battery costs and market,” *Bloomberg New Energy Finance*, vol. 5, pp. 4–6, 2017.
- [5] L. Goldie-Scot. (2019). “A behind the scenes take on lithium-ion battery prices,” [Online]. Available: <https://about.bnef.com/blog/behind-scenes-take-lithium-ion-battery-prices> (visited on 03/05/2019).
- [6] V. Henze. (2020). “Battery pack prices cited below \$100/kwh for the first time in 2020, while market average sits at \$137/kwh,” [Online]. Available: <https://about.bnef.com/blog/battery-pack-prices-cited-below-100-kwh-for-the-first-time-in-2020-while-market-average-sits-at-137-kwh> (visited on 12/16/2020).
- [7] D. Andrea, *Battery management systems for large lithium-ion battery packs*. Artech house, 2010.
- [8] H. Rahimi-Eichi, U. Ojha, F. Baronti, and M.-Y. Chow, “Battery management system: An overview of its application in the smart grid and electric vehicles,” *IEEE Industrial Electronics Magazine*, vol. 7, no. 2, pp. 4–16, 2013.
- [9] D. P. Kingma and J. Ba, “Adam: A method for stochastic optimization,” *arXiv preprint arXiv:1412.6980*, 2014.
- [10] M. Yoshio, R. J. Brodd, and A. Kozawa, *Lithium-ion batteries*. Springer, 2009, vol. 1.
- [11] J. Vetter, P. Novák, M. R. Wagner, C. Veit, K.-C. Möller, J. Besenhard, M. Winter, M. Wohlfahrt-Mehrens, C. Vogler, and A. Hammouche, “Ageing mechanisms in lithium-ion batteries,” *Journal of power sources*, vol. 147, no. 1-2, pp. 269–281, 2005.
- [12] A. Manthiram, “An outlook on lithium ion battery technology,” *ACS central science*, vol. 3, no. 10, pp. 1063–1069, 2017.

- [13] L. Lu, X. Han, J. Li, J. Hua, and M. Ouyang, “A review on the key issues for lithium-ion battery management in electric vehicles,” *Journal of power sources*, vol. 226, pp. 272–288, 2013.
- [14] L. Lavigne, J. Sabatier, J. M. Francisco, F. Guillemard, and A. Noury, “Lithium-ion open circuit voltage (ocv) curve modelling and its ageing adjustment,” *Journal of Power Sources*, vol. 324, pp. 694–703, 2016.
- [15] B. Haus and P. Mercorelli, “Polynomial augmented extended kalman filter to estimate the state of charge of lithium-ion batteries,” *IEEE Transactions on Vehicular Technology*, vol. 69, no. 2, pp. 1452–1463, 2019.
- [16] X. Hu, F. Feng, K. Liu, L. Zhang, J. Xie, and B. Liu, “State estimation for advanced battery management: Key challenges and future trends,” *Renewable and Sustainable Energy Reviews*, vol. 114, 2019.
- [17] B. Gou, Y. Xu, and X. Feng, “State-of-health estimation and remaining-useful-life prediction for lithium-ion battery using a hybrid data-driven method,” *IEEE Transactions on Vehicular Technology*, 2020.
- [18] J. Wu, C. Zhang, and Z. Chen, “An online method for lithium-ion battery remaining useful life estimation using importance sampling and neural networks,” *Applied energy*, vol. 173, pp. 134–140, 2016.
- [19] H. He, R. Xiong, and J. Fan, “Evaluation of lithium-ion battery equivalent circuit models for state of charge estimation by an experimental approach,” *energies*, vol. 4, no. 4, pp. 582–598, 2011.
- [20] X. Hu, F. Sun, and Y. Zou, “Estimation of state of charge of a lithium-ion battery pack for electric vehicles using an adaptive luenberger observer,” *Energies*, vol. 3, no. 9, pp. 1586–1603, 2010.
- [21] S. S. Madani, E. Schaltz, and S. K. Kær, “A review of different electric equivalent circuit models and parameter identification methods of lithium-ion batteries,” *ECS Transactions*, vol. 87, no. 1, p. 23, 2018.
- [22] B. Y. Liaw, G. Nagasubramanian, R. G. Jungst, and D. H. Doughty, “Modeling of lithium ion cells—a simple equivalent-circuit model approach,” *Solid state ionics*, vol. 175, no. 1-4, pp. 835–839, 2004.
- [23] Y. Zou, X. Hu, H. Ma, and S. E. Li, “Combined state of charge and state of health estimation over lithium-ion battery cell cycle lifespan for electric vehicles,” *Journal of Power Sources*, vol. 273, pp. 793–803, 2015.
- [24] B. Bole, C. Kulkarni, and M. Daigle, “Randomized battery usage data set,” *NASA AMES prognostics data repository*, vol. 70, 2014.
- [25] *Lithium-ion battery data sheet*, EEMB Co., Ltd., Nov. 2010.
- [26] Z. Wei, T. M. Lim, M. Skyllas-Kazacos, N. Wai, and K. J. Tseng, “Online state of charge and model parameter co-estimation based on a novel multi-timescale estimator for vanadium redox flow battery,” *Applied Energy*, vol. 172, pp. 169–179, 2016.

- [27] J. Schmidhuber, “Deep learning in neural networks: An overview,” *Neural networks*, vol. 61, pp. 85–117, 2015.
- [28] A. Abraham, “Artificial neural networks,” *Handbook of measuring system design*, 2005.
- [29] K. S. Ng, C.-S. Moo, Y.-P. Chen, and Y.-C. Hsieh, “Enhanced coulomb counting method for estimating state-of-charge and state-of-health of lithium-ion batteries,” *Applied energy*, vol. 86, no. 9, pp. 1506–1511, 2009.
- [30] C. Weng, J. Sun, and H. Peng, “A unified open-circuit-voltage model of lithium-ion batteries for state-of-charge estimation and state-of-health monitoring,” *Journal of power Sources*, vol. 258, pp. 228–237, 2014.
- [31] M. Galeotti, L. Cinà, C. Giammanco, S. Cordiner, and A. Di Carlo, “Performance analysis and soh (state of health) evaluation of lithium polymer batteries through electrochemical impedance spectroscopy,” *Energy*, vol. 89, pp. 678–686, 2015.
- [32] X. Wang, X. Wei, H. Dai, and Q. Wu, “State estimation of lithium ion battery based on electrochemical impedance spectroscopy with on-board impedance measurement system,” in *2015 IEEE Vehicle Power and Propulsion Conference (VPPC)*, IEEE, 2015, pp. 1–5.
- [33] X. Li, Z. Wang, and L. Zhang, “Co-estimation of capacity and state-of-charge for lithium-ion batteries in electric vehicles,” *Energy*, vol. 174, pp. 33–44, 2019.
- [34] X. Feng, C. Weng, X. He, X. Han, L. Lu, D. Ren, and M. Ouyang, “Online state-of-health estimation for li-ion battery using partial charging segment based on support vector machine,” *IEEE Transactions on Vehicular Technology*, vol. 68, no. 9, pp. 8583–8592, 2019.
- [35] Y. Tan and G. Zhao, “Transfer learning with long short-term memory network for state-of-health prediction of lithium-ion batteries,” *IEEE Transactions on Industrial Electronics*, vol. 67, no. 10, pp. 8723–8731, 2019.
- [36] A. Khalid, A. Sundararajan, I. Acharya, and A. I. Sarwat, “Prediction of li-ion battery state of charge using multilayer perceptron and long short-term memory models,” in *2019 IEEE Transportation Electrification Conference and Expo (ITEC)*, IEEE, 2019, pp. 1–6.
- [37] Y. Ma, L. Wu, Y. Guan, and Z. Peng, “The capacity estimation and cycle life prediction of lithium-ion batteries using a new broad extreme learning machine approach,” *Journal of Power Sources*, vol. 476, 2020.
- [38] H. Pan, Z. Lü, H. Wang, H. Wei, and L. Chen, “Novel battery state-of-health online estimation method using multiple health indicators and an extreme learning machine,” *Energy*, vol. 160, pp. 466–477, 2018.
- [39] A. Naha, S. Han, S. Agarwal, A. Guha, A. Khandelwal, P. Tagade, K. S. Hariharan, S. M. Kolake, J. Yoon, and B. Oh, “An incremental voltage difference based technique for online state of health estimation of li-ion batteries,” *Scientific Reports*, vol. 10, no. 1, pp. 1–11, 2020.

- [40] X. Tang, C. Zou, K. Yao, G. Chen, B. Liu, Z. He, and F. Gao, "A fast estimation algorithm for lithium-ion battery state of health," *Journal of Power Sources*, vol. 396, pp. 453–458, 2018.
- [41] J. Tian, R. Xiong, and Q. Yu, "Fractional-order model-based incremental capacity analysis for degradation state recognition of lithium-ion batteries," *IEEE Transactions on Industrial Electronics*, vol. 66, no. 2, pp. 1576–1584, 2018.
- [42] Y. Li, M. Abdel-Monem, R. Gopalakrishnan, M. Bercibar, E. Nanini-Maury, N. Omar, P. van den Bossche, and J. Van Mierlo, "A quick on-line state of health estimation method for li-ion battery with incremental capacity curves processed by gaussian filter," *Journal of Power Sources*, vol. 373, pp. 40–53, 2018.
- [43] L. Wang, C. Pan, L. Liu, Y. Cheng, and X. Zhao, "On-board state of health estimation of lifepo4 battery pack through differential voltage analysis," *Applied energy*, vol. 168, pp. 465–472, 2016.
- [44] L. Wang, X. Zhao, L. Liu, and C. Pan, "State of health estimation of battery modules via differential voltage analysis with local data symmetry method," *Electrochimica Acta*, vol. 256, pp. 81–89, 2017.
- [45] Q. Yu, R. Xiong, R. Yang, and M. G. Pecht, "Online capacity estimation for lithium-ion batteries through joint estimation method," *Applied Energy*, vol. 255, 2019.
- [46] X. Li, Z. Wang, and L. Zhang, "Co-estimation of capacity and state-of-charge for lithium-ion batteries in electric vehicles," *Energy*, vol. 174, pp. 33–44, 2019.
- [47] Z. Cui, N. Cui, C. Wang, C. Li, and C. Zhang, "A robust online parameter identification method for lithium-ion battery model under asynchronous sampling and noise interference," *IEEE Transactions on Industrial Electronics*, 2020.
- [48] X. Hu, H. Yuan, C. Zou, Z. Li, and L. Zhang, "Co-estimation of state of charge and state of health for lithium-ion batteries based on fractional-order calculus," *IEEE Transactions on Vehicular Technology*, vol. 67, no. 11, pp. 10 319–10 329, 2018.
- [49] W. Yan, B. Zhang, G. Zhao, S. Tang, G. Niu, and X. Wang, "A battery management system with a lebesgue-sampling-based extended kalman filter," *IEEE transactions on industrial electronics*, vol. 66, no. 4, pp. 3227–3236, 2018.
- [50] B. Pattipati, B. Balasingam, G. Avvari, K. Pattipati, and Y. Bar-Shalom, "Open circuit voltage characterization of lithium-ion batteries," *Journal of Power Sources*, vol. 269, pp. 317–333, 2014.
- [51] A. Farmann and D. U. Sauer, "A study on the dependency of the open-circuit voltage on temperature and actual aging state of lithium-ion batteries," *Journal of Power Sources*, vol. 347, pp. 1–13, 2017.
- [52] L. Wang, D. Lu, Q. Liu, L. Liu, and X. Zhao, "State of charge estimation for lifepo4 battery via dual extended kalman filter and charging voltage curve," *Electrochimica Acta*, vol. 296, pp. 1009–1017, 2019.

- [53] W. H. Press and S. A. Teukolsky, "Savitzky-golay smoothing filters," *Computers in Physics*, vol. 4, no. 6, pp. 669–672, 1990.
- [54] C. Hu, B. D. Youn, and J. Chung, "A multiscale framework with extended kalman filter for lithium-ion battery soc and capacity estimation," *Applied Energy*, vol. 92, pp. 694–704, 2012.
- [55] Z. Wei, J. Zhao, D. Ji, and K. J. Tseng, "A multi-timescale estimator for battery state of charge and capacity dual estimation based on an online identified model," *Applied energy*, vol. 204, pp. 1264–1274, 2017.
- [56] R. Xiong, F. Sun, Z. Chen, and H. He, "A data-driven multi-scale extended kalman filtering based parameter and state estimation approach of lithium-ion polymer battery in electric vehicles," *Applied Energy*, vol. 113, pp. 463–476, 2014.
- [57] Y. Xing, W. He, M. Pecht, and K. L. Tsui, "State of charge estimation of lithium-ion batteries using the open-circuit voltage at various ambient temperatures," *Applied Energy*, vol. 113, pp. 106–115, 2014.
- [58] D. Whitley, "A genetic algorithm tutorial," *Statistics and computing*, vol. 4, no. 2, pp. 65–85, 1994.
- [59] K. V. Price, "Differential evolution," in *Handbook of optimization*, Springer, 2013, pp. 187–214.
- [60] J. Kennedy and R. Eberhart, "Particle swarm optimization," in *Proceedings of ICNN'95-international conference on neural networks*, IEEE, vol. 4, 1995, pp. 1942–1948.
- [61] M. Dorigo, M. Birattari, and T. Stutzle, "Ant colony optimization," *IEEE computational intelligence magazine*, vol. 1, no. 4, pp. 28–39, 2006.
- [62] P. J. Van Laarhoven and E. H. Aarts, "Simulated annealing," in *Simulated annealing: Theory and applications*, Springer, 1987, pp. 7–15.
- [63] W. Zhang, W. Shi, and Z. Ma, "Adaptive unscented kalman filter based state of energy and power capability estimation approach for lithium-ion battery," *Journal of Power Sources*, vol. 289, pp. 50–62, 2015.
- [64] T. Feng, L. Yang, X. Zhao, H. Zhang, and J. Qiang, "Online identification of lithium-ion battery parameters based on an improved equivalent-circuit model and its implementation on battery state-of-power prediction," *Journal of Power Sources*, vol. 281, pp. 192–203, 2015.
- [65] P. Shen, M. Ouyang, L. Lu, J. Li, and X. Feng, "The co-estimation of state of charge, state of health, and state of function for lithium-ion batteries in electric vehicles," *IEEE Transactions on vehicular technology*, vol. 67, no. 1, pp. 92–103, 2017.
- [66] M. A. Hannan, M. M. Hoque, S. E. Peng, and M. N. Uddin, "Lithium-ion battery charge equalization algorithm for electric vehicle applications," *IEEE Transactions on Industry Applications*, vol. 53, no. 3, pp. 2541–2549, 2017.

- [67] S. W. Moore and P. J. Schneider, "A review of cell equalization methods for lithium ion and lithium polymer battery systems," 2001.

# Appendix A: Details of the Neural Network in Chapter 4

In this section, the details regarding the neural network used in Chapter 4 will be provided. As mentioned in Chapter 4, the inputs of the neural network are battery SOC, SOH, and temperature, and the target is the steady state internal resistance  $R_0 = R_p + R_s$ . In other words, the neural network is supposed to find the function  $R_0 = h(\text{SOC}, \text{SOH}, T)$ . Therefore, the size of the input layer is 3 and the size of the output layer is 1. The value of SOC and SOH are obtained from the reference measurements and the value of  $R_0$  is obtained from the estimation results achieved in Chapter 3. The structure of the neural network is depicted in Fig. A.1.

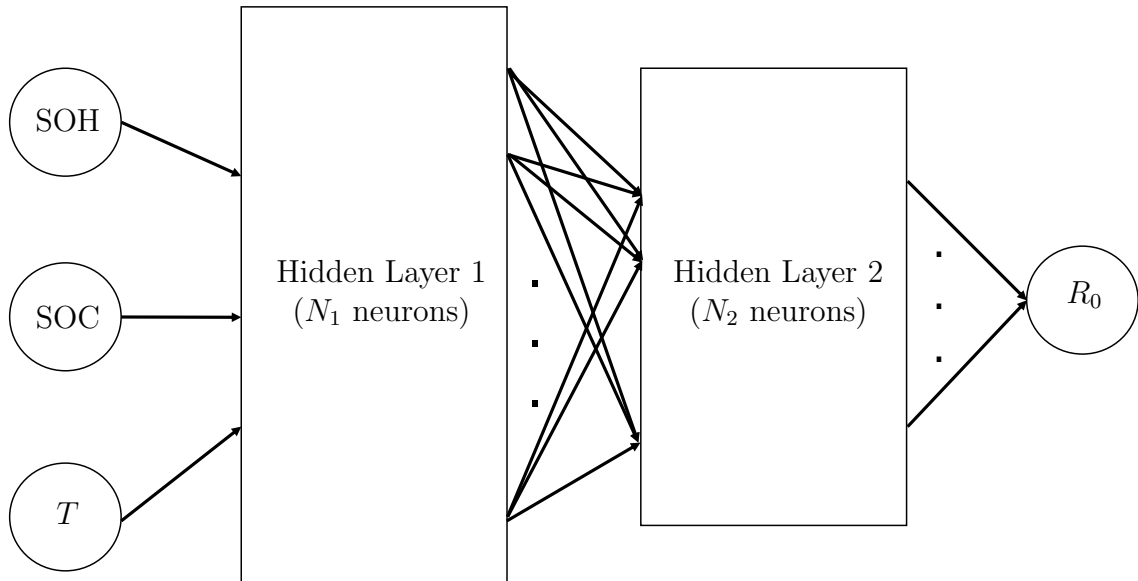


Figure A.1: Neural network's structure.

As can be seen in Fig. A.1, the network contains two hidden layers. The number of

neurons in each hidden layer are considered as the hyper-parameters and are obtained after performing cross validation on the training data, which will be explained later. Sigmoid is used as the activation function of the first hidden layer and relu is used as the activation function of the second hidden layer and the output layer.

Batteries B14 and B15 in NASA dataset are used here. Separate networks are trained for each of these batteries and after training, it is checked if these networks result in the same function. For each sample in the dataset, SOC, SOH, temperature, and  $R_0$  are extracted and used for training and validation of the neural network. Before training, a preprocessing on the inputs and the targets have been performed, in order to normalize their value between 0 and 1 to ensure fast convergence. The performance of the network is evaluated by the RMSE between the predicted values and the true values.

To find the optimum values of the hyper-parameters of each network, k-fold cross validation with k=5 is used. In other words, the training data are divided into 5 segments with equal lengths. For each set of hyper-parameters, a network is trained five times, each time with one of the segments used as the validation set and the rest as the training set. The resulting RMSEs are then calculated and their average is used as the RMSE of that set of hyper-parameters. The set of hyper-parameters that result in the smallest RMSE will be used as the selected network’s hyper-parameters. Table A.1 shows the trained parameters and results of the networks trained with batteries B14 and B15.

Table A.1: Summary of the parameters and results of the trained neural networks on batteries B14 and B15

	Training Samples	$N_1$	$N_2$	RMSE	$m [m\Omega/^\circ\text{C}]$
B14	1208698	9	3	0.023	-0.9
B15	1269639	10	3	0.025	-0.88

In Table A.1,  $N_1$  and  $N_2$  are the number of neurons in hidden layers, achieved by

k-fold cross validation and the reported RMSE values are the average RMSE on the validation sets for the selected hyper-parameters  $N_1$  and  $N_2$ . Also,  $m$  is the average slope of the internal resistance change with temperature. Since  $R_0$  was normalized to values between 0 and 1, a RMSE of 0.02 indicates about 2% amplitude error, which is good enough for the purpose of this study.